Water Research 194 (2021) 116953

Contents lists available at ScienceDirect

Water Research

journal homepage: www.elsevier.com/locate/watres

A quasi-Monte Carlo based flocculation model for fine-grained cohesive sediments in aquatic environments

Xiaoteng Shen [1,2,3], Mingze Lin [2], Yuliang Zhu [1,2,3,*], Ho Kyung Ha [4], Michael Fettweis [5], Tianfeng Hou [6,7,8], Erik A. Toorman [9], Jerome P.-Y. Maa [10], Jinfeng Zhang [11]

[1] Key Laboratory of Ministry of Education for Coastal Disaster and Protection, Hohai University, Nanjing 210098, China
[2] College of Harbour, Coastal and Offshore Engineering, Hohai University, Nanjing 210098, China
[3] Engineering Research Center of Ministry of Education for Dredging Technology, Hohai University, Nanjing 210098, China
[4] Department of Ocean Sciences, Inha University, Incheon 22212, Republic of Korea
[5] Operational Directorate Natural Environment, Royal Belgian Institute of Natural Sciences, Rue Vautier 29, 1000 Brussels, Belgium
[6] Prediction Science Laboratory, RIKEN Cluster for Pioneering Research, Kobe, Japan
[7] Data Assimilation Research Team, RIKEN Center for Computational Science, Kobe, Japan
[8] RIKEN iTHEMS, Wako, Saitama 351-0198, Japan
[9] Hydraulics Laboratory, Department of Civil Engineering, KU Leuven, Kasteelpark Arenberg 40, B-3001 Leuven, Belgium
[10] Virginia Institute of Marine Science, College of William & Mary, Gloucester Point, VA 23062, United States
[11] State Key Laboratory of Hydraulic Engineering Simulation and Safety, Tianjin University, Tianjin 300072, China

ARTICLE INFO

Article history:
Received 23 December 2020
Revised 17 February 2021
Accepted 18 February 2021
Available online 22 February 2021

Key words:
Cohesive sediments
flocculation
quasi-Monte Carlo
population balance model
floc size distribution

ABSTRACT

The quasi-Monte Carlo (QMC) method was enhanced to solve the population balance model (PBM) including aggregation and fragmentation processes for simulating the temporal evolutions of characteristic sizes and floc size distributions (FSDs) of cohesive sediments. Ideal cases with analytical solutions were firstly adopted to validate this QMC model to illustrate selected pure aggregation, pure fragmentation, and combined aggregation and fragmentation systems. Two available laboratory data sets, one with suspended kaolinite and the other with a mixture of kaolinite and montmorillonite, were further used to monitor the FSDs of cohesive sediments in controlled shear conditions. The model results show reasonable agreements with both analytical solutions and laboratory experiments. Moreover, different QMC schemes were tested and compared with the standard Monte Carlo scheme and a Latin Hypercube Sampling scheme to optimize the model performance. It shows that all QMC schemes perform better in both accuracy and time consumption than standard Monte Carlo scheme. In particular, compared with other schemes, the QMC scheme using Halton sequence requires the least particle numbers in the simulated system to reach reasonable accuracy. In the sensitivity tests, we also show that the fractal dimension and the fragmentation distribution function have large impacts on the predicted FSDs. This study indicates a great advance in employing QMC schemes to solve PBM for simulating the flocculation of cohesive sediments.

1. Introduction

Fine-grained cohesive sediments abound in open water systems such as estuaries, reservoirs, and coastal waters. The transport of cohesive sediments has great impacts on bed morphology, water quality, and estuarine circulations (Maggi, 2005; Edmonds and Slingerland, 2010; Geyer and MacCready, 2014; Burchard et al., 2018). One significant characteristic of cohesive suspended sediments is flocculation, which is the process where sediment particles go through aggregation and fragmentation simultaneously to form clusters (flocs). Accurate modeling flocculation of fine-grained sediments is still a challenge since the process is influenced by physical (e.g., turbulence intensity and sediment concentration), biological (e.g., Extracellular Polymeric Substances), and chemical (e.g., mineralogical composition, PH value, and salinity) effects (Tolhurst et al., 1999; Winterwerp, 1998; Tran and Strom, 2019; Azhikodan and Yokoyama, 2021; Fall et al., 2021).

Over the past decade, different kinds of flocculation models have been developed to track the sediment particle quantities. The first is the simplified Lagrangian model (sometimes also known as the floc growth model) developed by Winterwerp (1998) to track the evolution of a characteristic size under shear-dominated environments. Later, the constant fractal dimension (Maggi et al., 2007; Khelifa and Hill, 2006) and yield strength (Son and Hsu, 2009) in

* Corresponding author. Key Laboratory of Ministry of Education for Coastal Disaster and Protection, Hohai University, Nanjing 210098, China
E-mail address: zhuyl@hhu.edu.cn (Y. Zhu).

https://doi.org/10.1016/j.watres.2021.116953
0043-1354/

the Winterwerp's model were enhanced as a function of floc size, and the breakage parameter was connected with the Kolmogorov microscale (Kuprenas et al., 2018) to better address the effects of suspended sediment concentration on flocculation. This low-cost single class model can be easily adopted in real environments (e.g., Zhang et al., 2020); however, some properties of flocculation such as the effects of differential settling and the variations of bi- or multi-peak floc size distributions (FSDs) cannot be dealt with using the Winterwerp's model. The second flocculation model is the population balance model (PBM), which is a transport model based on an integro-partial differential equation that accounts for the number density of flocs with particular size at any location and time in a system. Although PBM has been widely used in many fields (e.g., aerosol, droplet, milling, and granulation), only few studies applied it to simulate FSDs for fine-grained cohesive sediments in natural environments (e.g., Maggi et al., 2007; Lee et al., 2011; Shen and Maa, 2015, 2016, 2017). Note that although the Winterwerp's model could be sometimes treated as a one-class PBM, here it is classified separately since the model cannot track the multi-modal distributions. Most of the other flocculation models mainly focused on the details of forces governing particle–particle interactions. For example, Zhang and Zhang (2011) extended the Lattice Boltzmann Model by adding fluid-solid boundary using bounce-back method to simulate the FSDs of cohesive sediments considering hydrodynamics and attractive van der Waals forces during differential settling, and their model was later applied under shear conditions as well (Zhang et al., 2013). In addition, Zhao et al. (2020) investigated the Stokes drag, lubrication, cohesive, and direct contact forces between particles, which performed well in the transient stage of flocculation in a conceptually simple and small cellular flow set-up. These models often consume exorbitant memory and computational resources, which limits themselves on studying large domains.

Among the above mentioned models, the population balance model (PBM) outperforms other models for its advantages in the ability of tracking FSDs and describing various flocculation mechanisms. Several numerical methods for solving PBM have been proposed, including discretization methods (Kumar and Ramkrishna, 1996; Bertin et al., 2016; Kumar and Kaur, 2016; Singh et al., 2019), moment methods (McGraw, 1997; Shen and Maa, 2015, 2016, 2017; Passalacqua et al., 2018; Li et al., 2019) and Monte Carlo (MC) methods (Khelifa and Hill, 2006; Xu et al, 2014; Lee et al., 2015; Das et al., 2020). The first approach, i.e., the discretization method, converts the PBM to a series of ordinary differential equations by discretizing the continuous number density function into several pivots to track the particle quantities (Singh et al., 2019). The disadvantage of this method is the requirement of large computing resources to obtain a desirable accuracy especially for cases with wide range of sizes (Shiea et al., 2020). The second approach, the methods of moments, was developed as an approximated solution that tracks the moments of the number density function and then reconstructs the number density function. The process of reconstructing the FSDs from their moments, however, may cost expensively in computing resource (Shen and Maa, 2015,2016; Li et al., 2019; Wang et al., 2020). The third approach, the Monte Carlo (MC) methods, deals with physical processes such as aggregation and fragmentation as discrete events by using probabilistic tools. With MC methods, one can conveniently obtain the time evolution of particle systems by using an array containing the particle size to represent a sample of the whole system and simulating the particulate behaviors, which makes it suitable for extension to multivariate (e.g., size, density, and biomass fraction) problems (Su et al., 2009; Zhao et al., 2011; Xu et al., 2014, Kotalczyk and Kruis, 2017). This capability of easy extension for finding other physical properties is our main motivation to use the MC method.

The MC methods for PBM can be classified into event-driven MC and time-driven MC by time discretization. In event-driven MC (Garcia et al., 1987), a specific event (e.g., aggregation and fragmentation) is first selected according to the probability that is proportional to the rate of its occurrence. The time increment is calculated for each event during the simulation. In the time-driven MC (Liffman, 1992), a specified time is first given less than the minimum time scale of all the possible events, and then all possible occurring events proceed within this pre-specified time. MC methods can also be divided into constant-volume MC and constant-number MC according to the simulated volume. The former keeps the system in a constant volume and thus changes the total number of particles but conserving the mass (Lin et al., 2002), while the latter adjusts the volume to keep the particles number unchanged. With the constant-volume MC, either the statistic error increases with time because of the reduction in particle number for aggregation events, or the computational cost increases due to the increasing particle number for fragmentation events. To balance the simulation efficiency and accuracy, the constant-number MC was developed to keep the particle number unchanged during the simulation by continuously adjusting the sampling volume (Tang and Matsoukas, 1997; Smith and Matsoukas, 1998).

The MC methods have rarely been applied to solve PBM for simulating the time evolution of FSDs for suspended sediments flocculation, except for some early studies by Khelifa et al. (2005, 2006). Although the MC methods have their superior discrete nature, the convergence rate of standard MC method can often be very slow, which costs more computational resources and time, especially for multivariate and high-dimensional problems (Caflisch, 1998; Wang and Sloan, 2011; Singhee and Rutenbar, 2010; Dick et al., 2013). Thus, a quasi-Monte Carlo (QMC) method was later developed by using quasi-random numbers (namely the low-discrepancy sequences) instead of standard MC's pseudorandom numbers (Radović et al., 1996; Sobol, 1998; Hou et al., 2019) to improve the efficiency and accuracy of standard MC. In this way, the QMC scheme for solving PBM has an optimal combination of high accuracy and efficiency.

The objective of this study is to simulate the temporal evolution of FSDs and characteristic sizes (e.g., mean size and median size) of fine-grained suspended sediments including aggregation and fragmentation using a modified quasi-Monte Carlo based PBM. In order to check the effectiveness of the model, data from (1) three analytical solutions given by Scott (1968), Ziff and McGrady (1985) and McCoy and Madras (2003) including pure aggregation, pure fragmentation, and combined aggregation and fragmentation systems, respectively, and (2) two laboratory experimental results from Tran and Strom (2017) and Maggi et al. (2002, 2007) are used for validations. Furthermore, the effectivity and efficiency of different QMC schemes are tested and compared with standard MC scheme to find the optimal model performance. The sensitivities on selected parameters are also discussed in order to investigate the model behavior.

This paper is organized as follows. Section 2.1 reviews the PBM model and explains the selection of inner functions in PBM. Section 2.2 presents the QMC schemes and describes the flocculation model. The model is thus calibrated and validated in section 3, with three analytical solutions and two laboratory experimental data sets. In the following, the discussion and conclusions are delivered in Section 4 and Section 5 respectively.

2. Flocculation model

2.1. Population balance model and sediment flocculation dynamics

The PBM model, neglecting the advection, diffusion and settling terms, is used to characterize aggregation and fragmentation dy-

namics to model the time evolutions of number density of flocs with size D. The size-based PBM in a continuous form can be written as (Marchisio et al., 2003b; Kariwala et al., 2012; Shen and Maa, 2016):

$$\frac{\partial n(D,t)}{\partial t} = \frac{D^2}{2}\int_0^D \frac{\beta\left(\left(D^3-\eta^3\right)^{\frac{1}{3}},\eta\right)\cdot\alpha\left(\left(D^3-\eta^3\right)^{\frac{1}{3}},\eta\right)}{\left(D^3-\eta^3\right)^{\frac{2}{3}}}\cdot n\left(\left(D^3-\eta^3\right)^{\frac{1}{3}},t\right)\cdot n(\eta,t)d\eta - n(D,t)\int_0^\infty \beta(D,\eta)\cdot\alpha(D,\eta)\cdot n(\eta,t)d\eta + \int_L^\infty a(\eta)\cdot b(D\eta)\cdot n(\eta,t)d\eta - a(D)\cdot n(D,t) \quad (1)$$

where $n(D,t)$ is the number density function of particles with size D at time t, $\beta(D,\eta)$ is the collision frequency for two particles of size D and η that collide to form a particle with size $(D^3+\eta^3)^{1/3}$, $\alpha(D,\eta)$ is the collision efficiency, $a(D)$ is the fragmentation frequency for particles with size D, and $b(D\eta)$ is the fragmentation distribution function that includes information on the daughter particles produced by fragmentation. The first term on the right-hand side of Eq. 1 is the birth rate of flocs with size D due to aggregation of smaller particles, the second term is the death rate of flocs with size D due to aggregation with other particles, the third term is the birth rate of flocs with size D due to fragmentation of bigger flocs with size η, and the last term is the death rate of flocs with size D due to their own fragmentation.

The collision efficiency α describes the probability of successful aggregation after collision between flocs. It is often used in the form of a calibration parameter (e.g., Mietta et al., 2008; Shen and Maa, 2015; Verney et al., 2011). The collision frequency β between sediment particles with size D_i and D_j in natural environments consists of three mechanisms: Brownian motion, differential settling, and turbulent shear. These terms can be written as (Smoluchowski, 1917; Maggi, 2005; Shen and Maa 2015)

$$\beta_{i,j} = \beta_{i,j}^{(BM)} + \beta_{i,j}^{(DS)} + \beta_{i,j}^{(TS)} \quad (2)$$

in which

$$\text{Brownian motion } \beta_{i,j}^{(BM)} = \frac{2}{3}\frac{KT}{\mu}\frac{\left(D_i+D_j\right)^2}{D_iD_j} \quad (3)$$

$$\text{Differential settling } \beta_{i,j}^{(DS)} = \frac{\pi}{4}\left(D_i+D_j\right)^2\left|\omega_{s,i}-\omega_{s,j}\right| \quad (4)$$

$$\text{Turbulent shear } \beta_{i,j}^{(TS)} = \frac{G}{6}\left(D_i+D_j\right)^3 \quad (5)$$

where K is the Boltzmann constant, T is the absolute temperature, μ is the dynamic viscosity of the fluid, $\omega_{s,i}$ and $\omega_{s,j}$ are the settling velocities of particles i and j, and G is the shear rate. Although Brownian motion is commonly known as a negligible factor in estuaries region (McCave, 1984; Winterwerp, 1998; Shen et al., 2018b), it is considered in this study for a complete expression.

The fragmentation frequency function $a(D)$ accounts for the disruption of flocs by stress produced by fluid shear and collision between flocs. The relative importance of these two influences are still debatable and not well understood (Khelifa and Hill, 2006; Shen and Maa, 2015). Models for floc fragmentation often employ complicated functions with fitting parameters (Winterwerp, 1998, 1999; Maggi et al., 2007; Shen and Maa, 2015, 2017). It is important to note that the probability of fragmentation of particles can be easily related to the floc size (Khelifa and Hill, 2006). A common kinematic approach regarding floc breakage defines a maximal floc size $D_{\max}$ instead of specifying the mechanism for fragmentation, which assumes that overlarge (i.e., larger than $D_{\max}$) flocs always tend to break into fragments. The fragmentation distribution function $b(D\eta)$ describes the number and size of daughter flocs after fragmentation. The assumptions used in this function are the discrete (e.g., binary breakup with mass ratio 1:1 or ternary breakup with mass ratio 1:1:2, see Spicer and Pratsinis, 1996; Shen, 2015) and the continuous form (e.g., Gaussian distribution).

2.2. Monte Carlo and Quasi-Monte Carlo

In this study, the constant-number MC method is applied in order to keep constant statistic accuracy over the simulation (Lin et al., 2002). As described in Fig. 1, random number generation (RNG) is the first step to produce a series of random numbers. The input parameters are the particles number (N), the maximum size ($D_{\max}$) of flocs, the turbulent energy dissipation rate, and the densities of solid particles (ρ_s) and of the fluid (ρ_w). The initial size distribution (ISD), fractal dimension (nf), and the fragmentation distribution function were selected before the events module. The initial particle array is filled randomly with a specific size distribution (e.g., Gaussian distribution and uniform distribution). The fractal dimension (nf) of flocs are given by (Maggi et al., 2007)

$$nf = 3\cdot\left(\frac{D_f}{D_p}\right)^{\delta} \quad (6)$$

where D_p is the primary particle size, and $\delta = -0.1$ is used as suggested by Maggi et al. (2005). The floc size, D_f, is converted to component particle numbers, N_f, to better track and conserve the mass, similar as proposed by Maggi (2005) and Khelifa and Hill (2006):

$$N_f = \left(\frac{D_f}{D_p}\right)^{nf} \quad (7)$$

The next step is choosing the aggregation or fragmentation events. Since little is known about the occurrence rate of the fragmentation, the following probability P_{frag} of floc breakage based on the number of overlarge flocs (larger than $D_{\max}$) is used as suggested by Khelifa and Hill (2006):

$$P_{\text{frag}} = \begin{cases} 0, & n_b = 0 \\ 0.5, & n_b = 1 \\ 1, & n_b > 1 \end{cases} \quad (8)$$

where n_b is the number of overlarge flocs. The aggregation probability is $P_{\text{agg}} = 1 - P_{\text{frag}}$ since the null event is not considered in the simulation. A random number r_1 is taken from the random number series which is produced before simulating. The aggregation event is selected if $P_{\text{frag}} < r_1$, otherwise the fragmentation event is selected.

The acceptance-rejection (AR) method is applied in the implementation of each selected event. Two random particles i and j are selected and their aggregation kernel $A_{ij} = \alpha_{i,j}\bullet\beta_{i,j}$ is calculated by Eqs. 2~5 with a constant $\alpha = C_1$ for the aggregation event. Here, the collision efficiency α is set as unity, which raises the flocculation rate while reasonably maintaining the feature of floc size distributions (Khelifa and Hill, 2006). This selection based on the assumption that α does not significantly depend on floc properties (e.g., size, shape, and biomass fraction) in our cases; nevertheless, the α shall be more challenging in QMC models if the biomass fraction is highlighted in natural waters (Kiørboe et al., 1990; Lai et al., 2018). A random number r_2 is taken from the random number series produced before the simulation. The pair of selected particles i and j would aggregate to a floc containing $N_{fi} + N_{fj}$ component particles (Fig. 1) if the aggregation kernel A_{ij} satisfies the following condition (Khelifa and Hill, 2006; Zhao and Zheng, 2013; Kotalczyk and Kruis, 2017):

$$r_2 \le A_{ij}/A_{\max} \quad (9)$$

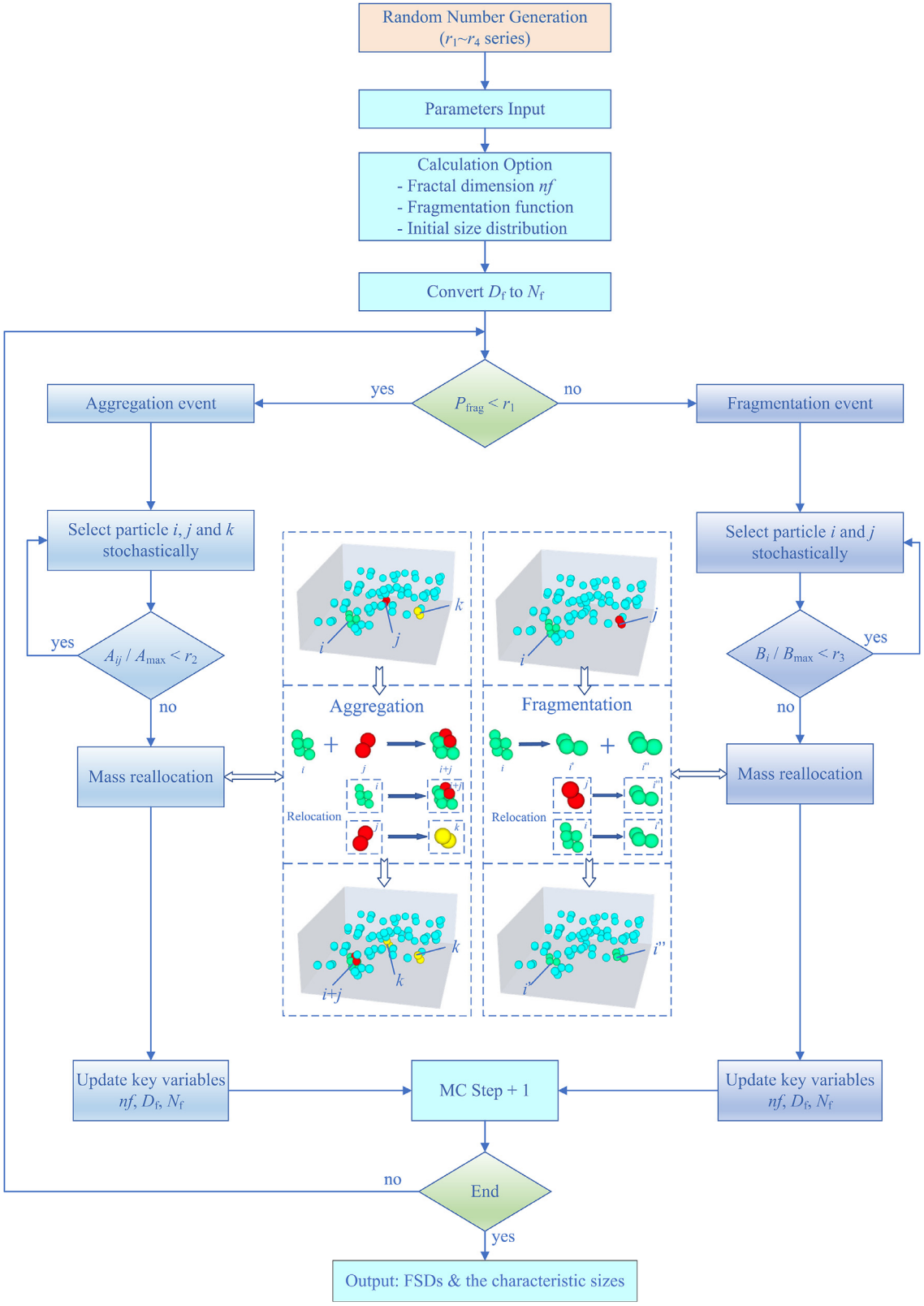

Fig. 1. The flowchart of the QMC model for cohesive sediment flocculation due to aggregation and fragmentation.

where A_{max} is the maximum of the aggregation kernel over all possible pairs. After a successful aggregation, the new formed floc is stored in the position of particle *i*. Then the position vacated by particle *j* is occupied by a duplicated particle of randomly selected particle *k*. If Eq. 9 is not satisfied, a new pair of particles is selected and the procedure is repeated until a pair of particles successfully aggregates.

Note that the calculation of the maximum aggregation kernel A_{max} requests a double looping over all pairs of particles in each step, which computes expensively $N(N\text{-}1)/2$ times for every try. A

simple constant maximum kernel may be used to reduce the calculation time as proposed by Smith and Matsoukas (1998), which is computationally feasible but not efficient in practical application for cohesive sediments. Kruis et al. (2000) introduced a so-called bookkeeping strategy that calculates the aggregation kernels of all pairs of particles first and only updates the kernel of which particle size is changed after each event. Eibeck and Wagner (2001) and Xu (2014) proposed a differential weight MC (DWMC) which used the majorant of the aggregation kernel to calculate the $A_{\max}$ by a single looping over all particle pairs instead of double looping. Although both the bookkeeping strategy and DWMC cost less CPU time than a traditional double looping strategy, they still consume much time when the particle number N is large. Khelifa and Hill (2006) proposed an automatically adjusted correction factor C_F to estimate the $A_{\max}$ by multiplying with the kernel of the mean size of flocs, which is validated with in-situ data of FSDs of cohesive sediments. Thus, the $A_{\max}$ is estimated as

$$A_{\max} = C_F A_{\text{mean}} \tag{10}$$

with

$$C_{\text{F}} = \frac{4n_a}{n_r + n_a} \tag{11}$$

where A_{mean} is the aggregation kernel of flocs with mean size, and n_a and n_r are the number of accepted and rejected tries respectively during each aggregation event. It is critical to note that the linear variation of C_F tends to remain the ratio n_a: n_r close to one and the calculation of $A_{\max}$ in Eq. 10 implies an assumption that $A_{\max} \sim 2A_{\text{mean}}$ in the simulation.

In the case of a fragmentation event, a particle i is selected randomly from the array. The acceptance-rejection (AR) method is also used to test the breakup probability with $B_i = N_{fi} / N_{\max}$. A random number r_3 from the pre-produced series is taken. If $B_i \geq r_3$, the particle i breaks into daughter flocs. Taking binary fragmentation as an example (Fig. 1), a random number r_4 is taken from the series produced already. The particle i breaks into two fragments i' with $r_4 \cdot N_{fi}$ component particles and i'' with $(1-r_4) \cdot N_{fi}$ component particles as follows:

$$\begin{cases} N_{fi'} = r_4 N_{fi} \\ N_{fi''} = (1 - r_4) N_{fi} \end{cases} \tag{12}$$

The daughter particle i' is placed in the position of particle i, while the particle i'' replaces a particle in the system stochastically.

After each step of aggregation or fragmentation, those key variables such as nf, D_f, N_f of changed particles will be updated. The simulation will be terminated when equilibrium has been reached. The FSDs and the characteristic sizes can be directly computed from the particle array.

Although the standard Monte Carlo method using pseudorandom numbers shows an advantage of discrete nature for solving PBM, it needs to be enhanced due to the huge computation cost. Thus, quasi-Monte Carlo schemes are developed to improve the performance of standard MC by substituting the pseudorandom numbers by quasi-number sequences (Singhee and Rutenbar, 2010; Dick et al., 2013; Hou et al., 2019), namely the deterministic low-discrepancy sequences, which show more uniformity in distribution. Two different quasi-number sequences, the Halton sequence (Halton, 1960) and the Sobol' sequence (Sobol, 1967), will be used in this numerical study. The Halton sequence is the first class of low-discrepancy sequences constructed in 1960 by Halton, which was frequently selected to substitute pseudorandom numbers in standard MC due to its good performance and simplicity (Wang and Hickernell, 2000; Hess and Polak, 2003; Mascagni and Chi., 2004; Chi et al., 2005). The Sobol' sequence belongs to a new class of sequences called LP_τ-sequences introduced in 1966, which has additional uniformity properties and can be computed in a "superfast" way using logical operations (Sobol, 1998; Burhenne et al., 2011).

Besides, the Latin Hypercube Sampling (LHS) sequence (McKay and Beckman, 1979) as a classic low-discrepancy sequence is also tested. The LHS is suggested as a particular kind of stratified sampling to improve the efficiency of different sampling methods and used to be an alternative of standard MC numbers in many research fields such as finite element analysis, structural reliability, and statistical circuit analysis (e.g., Keramat and Kielbasa, 1997; Olsson et al., 2002, 2003; Singhee and Rutenbar, 2010).

In order to better assess the uniformity of different sequences, 1000 points generated by each of four random number sequences are scatter-plotted in Fig. 2. One can easily see that the pseudo-random number and LHS sequences has more gaps and clumps than the other two sequences. In other words, the Halton sequence and the Sobol' sequence distribute visually more uniform than the others. For the purpose of qualifying the uniformity of these sequences, we define an area ratio index for the scatter-plot (Fig. 2) as

$$r_a = \frac{A_{\text{seq}}}{A_{\text{all}}} \tag{13}$$

where A_{seq} is the summed area in the image taken by all the markers of each points sequence, A_{all} is the whole area enclosed by the coordinates $x = 0$ to 1 and $y = 0$ to 1 (in this case). The value of index r_a is between 0 to 1, and $r_a = 1$ denotes that the sequence is uniformly distributed. In this study, the radius of each marker is empirically set to 20 pounds, and thus A_{seq} can be calculated using image processing tools. As shown in Fig. 2, the area ratio index r_a shows that not only the pseudorandom number series is less geometrically uniform than the low-discrepancy series but the uniformity of the Sobol' and Halton sequences are also of a higher level than others. The efficiency and accuracy of all four sequences-based MC method to solve PBM will be discussed later in Section 4.1.

3. Case study

In the following cases, all simulations were performed with $N = 30{,}000$ particles, which will be discussed in more details in section 4. Simulations were run for 5×10^5 MC steps. Temperature and the dynamic viscosity of the water were kept constant at 20 °C and 0.001 Pa·s. The density of the water and component particles were set to 1020 kg/m^3 and 2650 kg/m^3 respectively.

3.1. Comparison with selected analytical solutions

Case I: Pure aggregation

Based on the assumption that aggregation between particles is totally at random, a constant aggregation kernel is considered, which indicates that each pair of selected particles (i, j) is always aggregated after collision. With the simple assumption of Eq. 14,

$$\beta_{i,j} = \beta_0 \tag{14}$$

the analytical solution of the PSD for this case is given by Scott (1968) as

$$n(D,t) = \frac{12 N_0 D^2}{v_0 (T_a + 2)^2} e^{-\frac{2D^3}{v_0 (T_a+2)}} \tag{15}$$

The initial particle distribution is specified as $T_a = 0$ in Eq. 16

$$n(D) = \frac{3N_0}{v_0} D^2 e^{-\frac{D^3}{v_0}} \tag{16}$$

in which N_0 is the initial total number of particles per unit volume (in units of m^{-3}), v_0 is the mean volume of the particles at the beginning (in units of m^{-3}), and $T_a = N_0\ \beta_0\ t$ is dimensionless time.

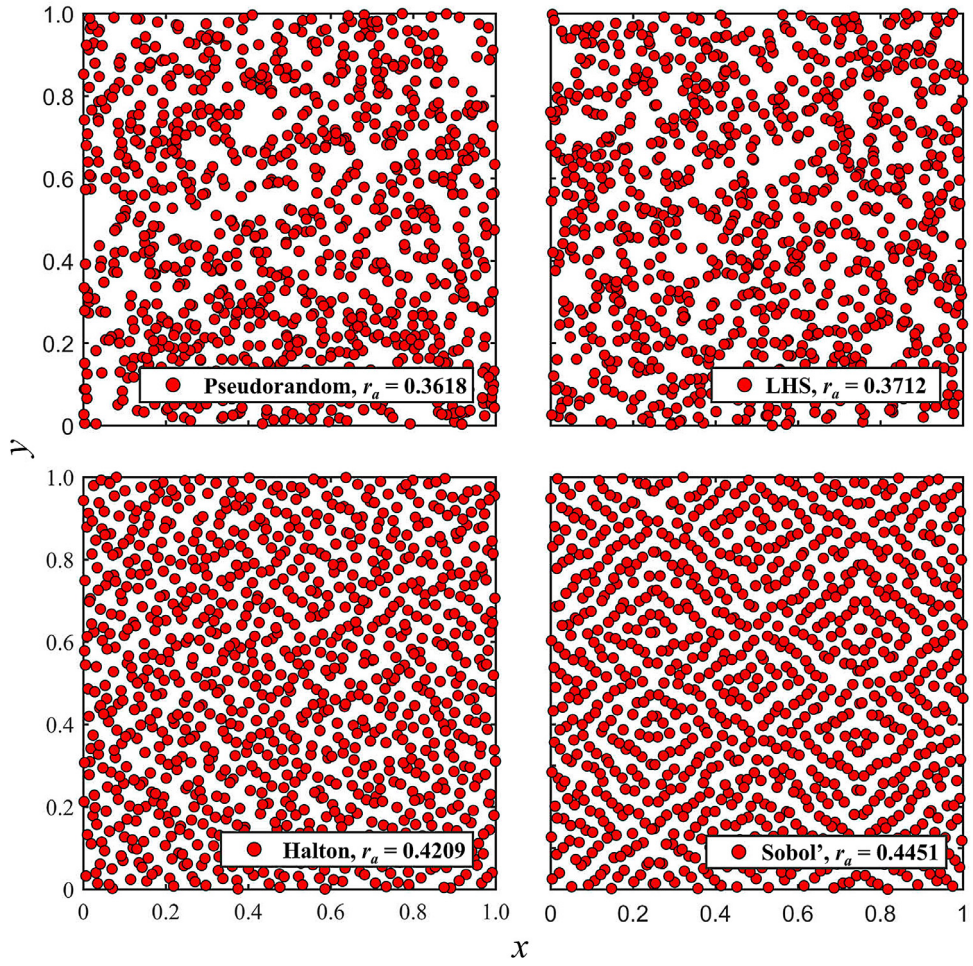

Fig. 2. Scatter plot of different sampling schemes with each of 1000 points. Top left is the results of pseudorandom (standard MC) approach, top right is Latin hypercube sampling, bottom left is Halton sequence, and bottom right is Sobol' sequence.

Since the constant-number MC and the event-driven MC were applied in this study, the inter-event time need to be computed while running the model. Smith and Matsoukas (1998) gave the time increment of aggregation as

$$\Delta t_\kappa = \frac{2\tau_c}{\langle \beta_{ij} \rangle} \cdot \frac{1}{N} \cdot \left(\frac{N}{N-1} \right)^\kappa \tag{17}$$

with

$$\tau_c = 1/\beta_C C_0 \tag{18}$$

where Δt_κ is the time increment (in units of s), κ is the counter of successful aggregation events, τ_c is the characteristic aggregation time, β_C is the dimensional part of the aggregation kernel (in units of m^3/s) which equals to β_0 in this case, and C_0 is total particle number concentration at the beginning. In addition, $<\beta_{ij}>$ is the ensemble average kernel, which can be written as a discrete form, namely

$$\langle \beta_{ij} \rangle = \frac{\sum_i^N \sum_{j \neq i}^N \beta_{ij}}{N(N-1)} \tag{19}$$

All of the constants are selected the same as those of earlier researches on the purpose of comparing the model results with these earlier studies. For instance, $C_0 = N_0 = 1$, $v_0 = 1$, and $<\beta_{ij}> = \beta_C = \beta_0 = 1$ are used in this study to match those of Shen and Maa (2016). Note that the analytical solution is a general formulation, the units of those parameter such as D, N_0 and v_0 in Eq. 15∼16 are not important and only require consistency.

The cumulative time t can be derived from Eq. 17 as

$$t = \sum_{\kappa=1}^{\kappa} \Delta t_\kappa = 2\left(\left(\frac{N}{N-1} \right)^\kappa - 1 \right) \tag{20}$$

Since the initial particle size distribution cannot be fitted perfectly with the discrete character of Monte Carlo method, the initial FSD calculated by analytical solution is divided into 1500 size classes and fitted approximately with $N = 30{,}000$ particles. In order to simplify the computation, the particle size at the peak concentration at $t = 0$ is selected as the primary particle size, i.e., $D_p = 0.87$ (in arbitrary length units), as inputs of the model in this case.

The predicted and analytical FSDs fit well with at $t = 0$, 10, 20, 50, 100, 200, and 300 s (Fig. 3). One can easily calculate the arithmetic mean size (mean of number-based FSD) of the analytical solution given as (Shen and Maa, 2016)

$$D_{mn} = \frac{\int_0^\infty Dn(D,t)dD}{\int_0^\infty n(D,t)dD} \tag{21}$$

by integral calculation. The simulated mean size also matches well with those given by analytical solution of the FSD (Fig. 3).

To better evaluate the progress of aggregation of a system, Marchisio et al. (2003a), gave an index $I_a = 1 - m_0(t)/m_0(0)$ to show the degree of aggregation, and Scott (1968) gave the analytical solution for all the moments, as

$$m_k(t) = m_k(t=0) \cdot \left(\frac{2}{2 + N_0 \beta_0 t} \right)^{1-\frac{k}{3}} \tag{22}$$

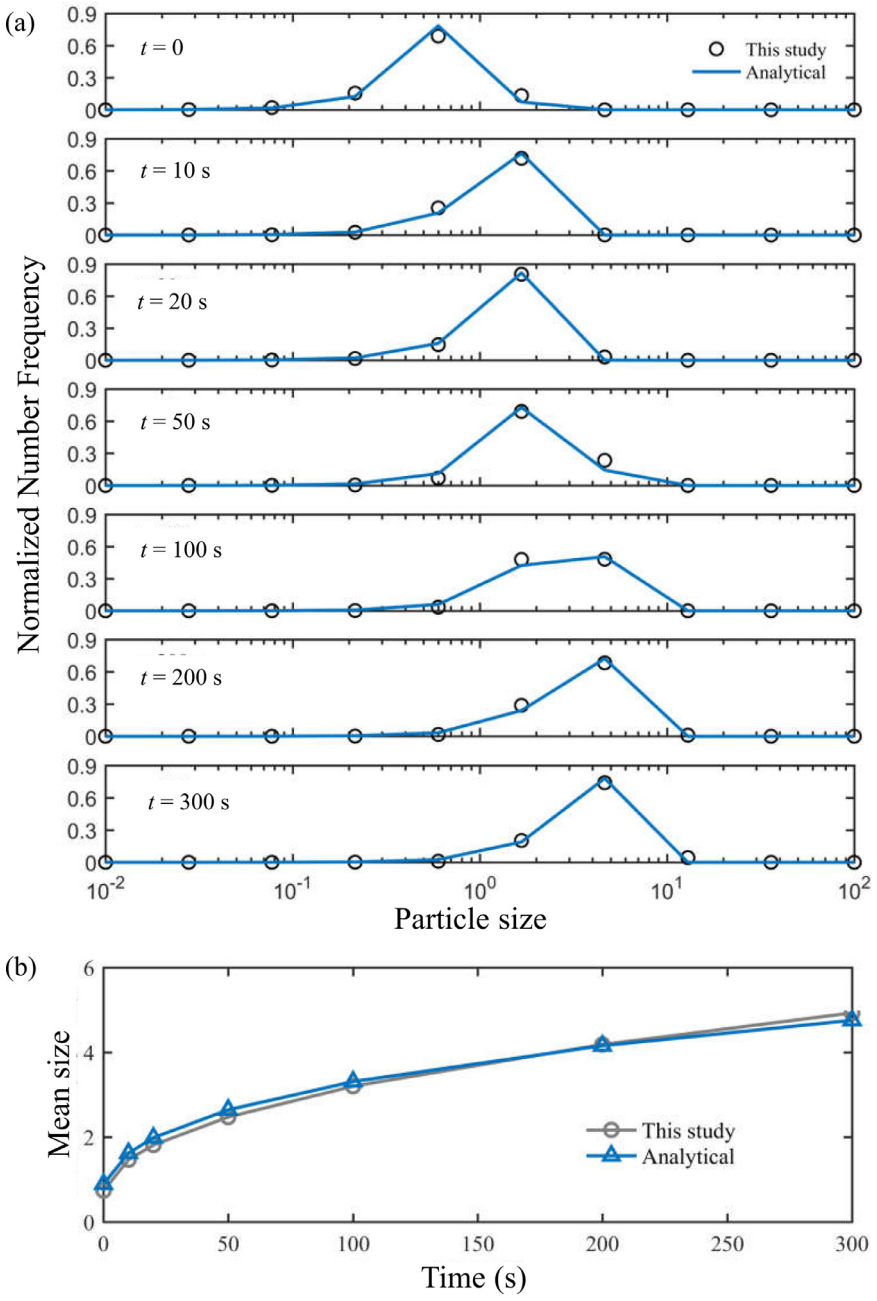

Fig. 3. Time evolution of (a) normalized PSDs and (b) mean sizes for the pure aggregation event with a constant aggregation kernel (Case I)

where $m_k(t)$ is the kth moments of FSD at time t. In this case, $m_0(0) = \int_0^\infty n(D,0)dD = 1$. Here $I_a = 0$ indicating no aggregation, and $I_a = 1$ denotes aggregation progresses in full pace. The relative error for mean size between simulated and the analytical result is less than 13% even at $t = 1000$ s, and the calculated $I_a = 99.8\%$ for the system at that time indicates that aggregation is still in progress with full pace.

Case II: Pure fragmentation

We consider the population balance model for a power breakup kernel as

$$a(D) = a_0 D^3 \tag{23}$$

where $a_0 = 1$ together with a uniform fragmentation distribution given by Su et al. (2008) as

$$b(D\lambda) = \frac{(6D^2)}{\lambda^3},\ 0 < D < \lambda \tag{24}$$

Limited by the nature of discretion of MC method, the chosen floc will break into two classes j and k. Each of that includes two daughter flocs of the same size. The size of daughter flocs is decided by a random number r_4 as

$$\begin{cases} N_{fj1} = N_{fj2} = r_4 N_{fi} \\ N_{fk1} = N_{fk2} = N_{fi}(1 - 2r_4)/2 \end{cases} \tag{25}$$

The time interval Δt_κ of the counter of successful fragmentation events κ, is given by Tang and Matsoukas (1997) as

$$\Delta t_\kappa = \frac{1}{\langle K_i \rangle} \cdot \left(1 - \frac{M_\kappa}{M_{\kappa-1}}\right) \tag{26}$$

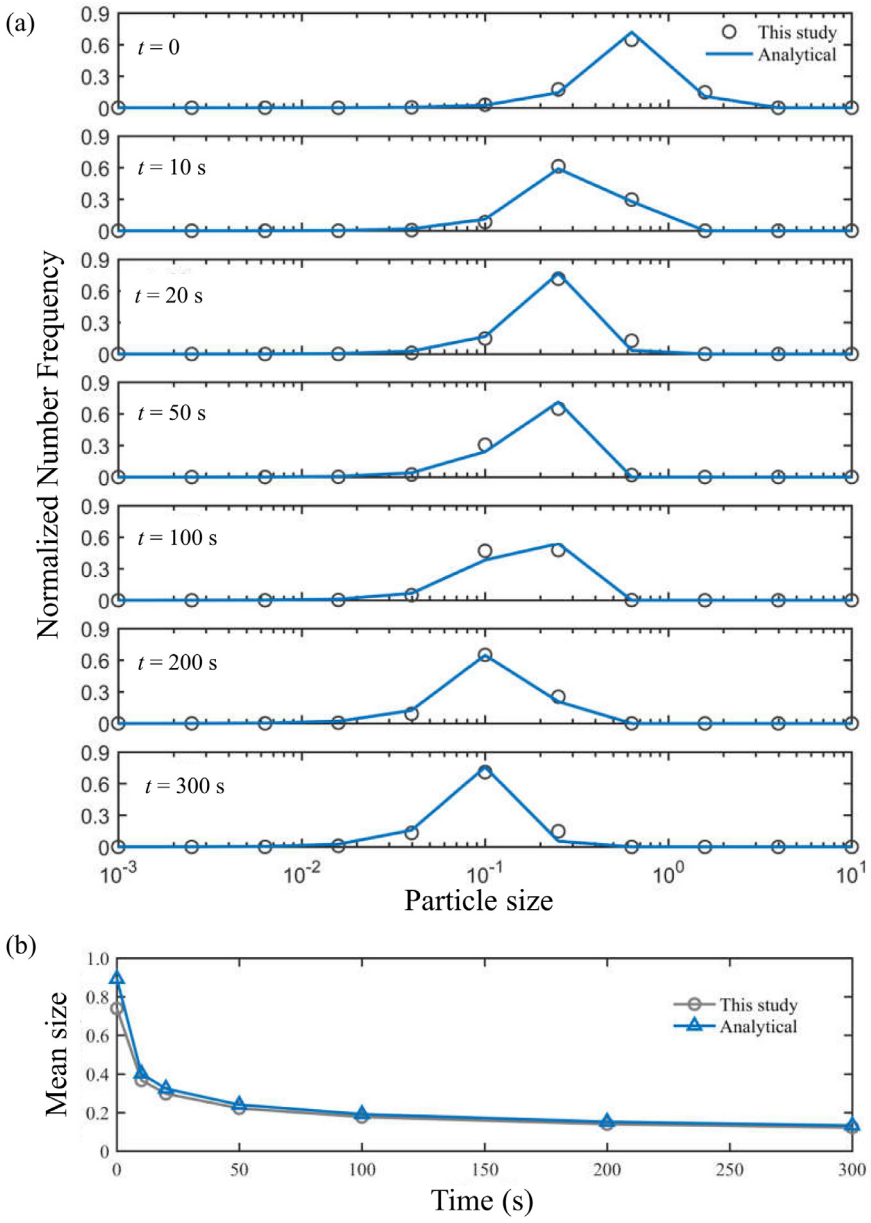

Fig. 4. Time evolution of (a) normalized PSDs and (b) mean sizes for the pure fragmentation event with a power law fragmentation kernel. (Case II)

where $<K_i> = \sum_i^N K_i/N$ is the mean fragmentation rate, and $M_{\kappa-1}$ and M_κ are the average mass before and after the κ fragmentation event. In order to reduce the computational resource, the average mass is estimated by the mass of the particle with average size.

The analytical solution of the FSD was given by Ziff and McGrady (1985) with the power initial distribution (Eq. 16) for this pure fragmentation case as follows

$$n(D,t) = \frac{3D^2N_0}{v_0}(1+a_0v_0t)^2e^{-\frac{D^3}{v_0}(1+a_0v_0t)} \tag{27}$$

In this case, we considered $N_0 = 1$ and $v_0 = 1$ following Shen and Maa (2016). It can be seen in Fig. 4 that all of FSDs at selected time and mean size obtained by model coincide with the analytical solution. The mean size and the peak size decrease quickly with the progression of fragmentation in the first ten seconds and the rate of reduction is slowing down with time. In addition, the maximum relative errors of mean size between analytical solution and the MC model at selected time is less than 9%.

One should be aware that Case I and Case II are rarely possible for cohesive sediments in natural waters, since aggregation and fragmentation are often co-existing. Flocs do not unlimited grow or decay. But these two cases were simulated to show that the QMC model works well under pure aggregation and pure fragmentation conditions, as pre-steps to validate true cohesive sediment cases. The results of Case I and Case II illustrate that the constant-number QMC scheme, compared to the previous constant-volume QMC scheme, maintains stable statistical accuracy when particles aggregate and requires reasonable memory when particles break up.

Case III: Combined aggregation and fragmentation

For the combined aggregation and fragmentation case, McCoy and Madras (2003) obtained a solution of the FSD for a constant aggregation kernel (Eq. 14 with a constant β_0), a power breakage kernel (Eq. 23 with a constant a_0), a uniform fragmentation distribution function (Eq. 24∼25), and an exponent

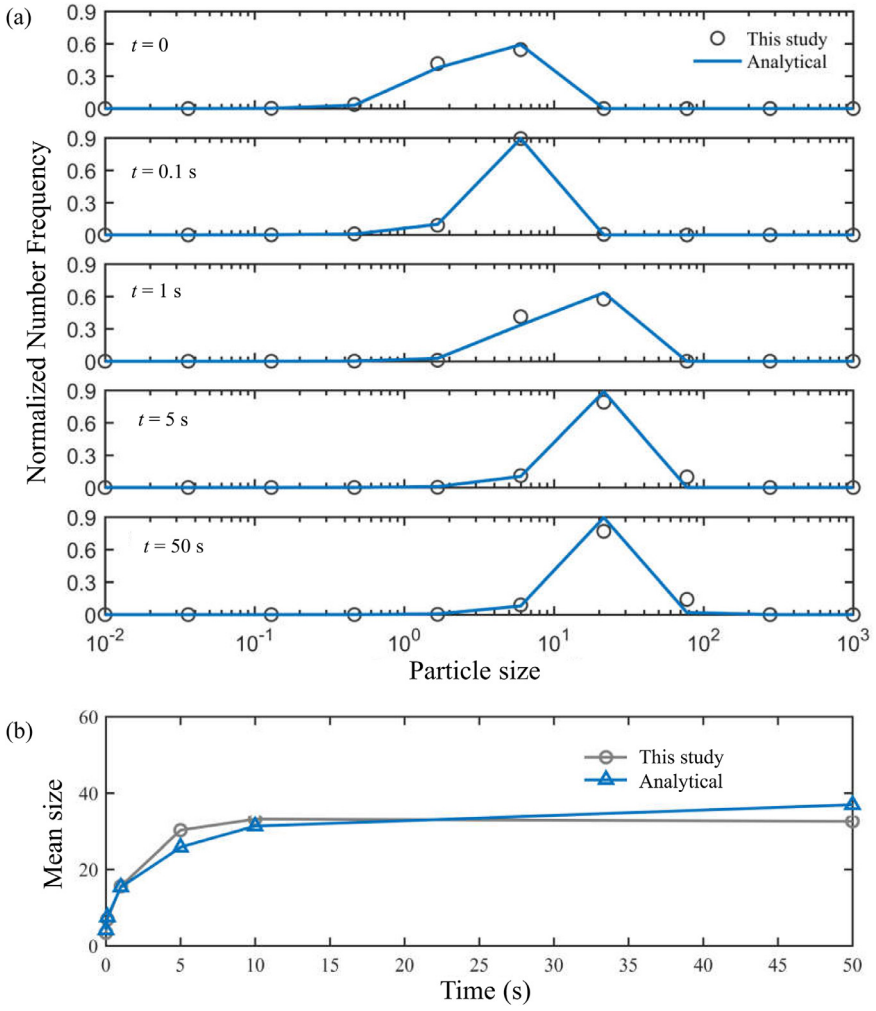

Fig. 5. Time evolution of (a) normalized PSDs and (b) mean sizes for the combined aggregation and fragmentation events with a constant aggregation kernel and a power law fragmentation kernel. (Case III)

initial distribution (Eq. 16) with the analytical FSD given by

$$n(D,t) = \frac{3N_0^2}{v_0} D^2 [\Phi(T_a)]^2 e^{-\frac{N_0}{v_0} D^3 \Phi(T_a)} \tag{28}$$

and the total number fraction at T_a follows

$$\Phi(T_a) = \frac{\Phi(\infty) \cdot \left[1 + \Phi(\infty) \cdot \tanh\left(\Phi(\infty) \cdot \frac{T_a}{2}\right)\right]}{\Phi(\infty) + \tanh\left(\Phi(\infty) \cdot \frac{T_a}{2}\right)} \tag{29}$$

where $\Phi(\infty) = (2a_0 v_0 N_0/\beta_0)^{0.5}/N_0$.

The time increment of a chosen event is calculated by Eq. 17 and Eq. 26. Fig. 5 presents the comparison of FSD and the mean size between the analytical solution and the model with those constants selected as $\beta_0 = 100$ in Eq. 14, $a_0 = 1 \times 10^{-6}$ in Eq. 23, and $N_0 = 1$, $v_0 = 100$ in Eq. 26 (Shen and Maa, 2016). The system reached an equilibrium state under the selected conditions after around fifty seconds. It can be observed that the model results at all time match quite well with the analytical solution. The aggregation process plays a leading role in the first 10 seconds and the mean size increases quickly. Then the fragmentation processes start to occur more frequently and the system reaches a steady state.

3.2. Comparison with experimental data

Case IV: Tran's mixing chamber experiment

Tran and Strom (2017) conducted a laboratory experiment to explore the interaction between clays and silts under turbulent shear conditions. The experiments were carried out in a mixing chamber of $27.5 \times 27.5 \times 25$ cm³, in which a variable speed paddle mixer was set to generate different magnitudes of turbulent shear. The pure clay sample consisted of a mixture of 80% kaolinite and 20% montmorillonite to mimic estuarine mud (Keyvani and Strom, 2014) and the concentration was maintained constant at 100 mg/L. Floc images were recorded by a camera system with a LED in a waterproofed housing placed inside the mixing tank. The field of camera view was 2.4×1.4 mm² with an image resolution of 1.3 μm/pixel. The pure clay suspension was sonicated for 15 min to break down large clay aggregates and to obtain an average initial size distribution around 5 μm. Then the suspension was introduced to clearwater fluid and mixed at $G = 50$ s^{-1} and $G = 95$ s^{-1} respectively. The initial particle distribution obeys a Gaussian distribution with mean D_p and standard deviation $D_p/3$. The maximum floc size was selected as the maximum value between the Kolmogorov scale and the 95th percentile D_{95}. Besides, the quantity and sizes of daughter flocs due to breakage of bigger flocs are logically and simply described by binary fragmentation at current stage (e.g., Khelifa and Hill, 2006; Lee and Molz, 2014; Mietta et al., 2011; Verney et al., 2011). Other aggregation and breakage fitting parameters are given in Table. 1.

Table. 1
The modeling parameters for each experiment, in which λ is the Kolmogorov length scale, D_{max} is the maximum floc size, and δ is the coefficient in Eq. 32.

Case	N	D_{max} (μm)	D_p (μm)	nf	$B(D\|\eta)$
Tran's experiment, $G=50$ s^{-1}	30000	416	5.0	2.2	Binary
Tran's experiment, $G=95$ s^{-1}	30000	258	5.0	2.2	Binary
Maggi's experiment, $G=10$ s^{-1}	30000	316	2.0	δ=-0.1	Binary
Maggi's experiment, $G=40$ s^{-1}	30000	158	2.0	δ= -0.1	Binary
Maggi's experiment, $G=5$ s^{-1}	30000	447	2.0	δ= -0.1	Binary
Maggi's experiment, $G=20$ s^{-1}	30000	223	2.0	δ= -0.1	Binary

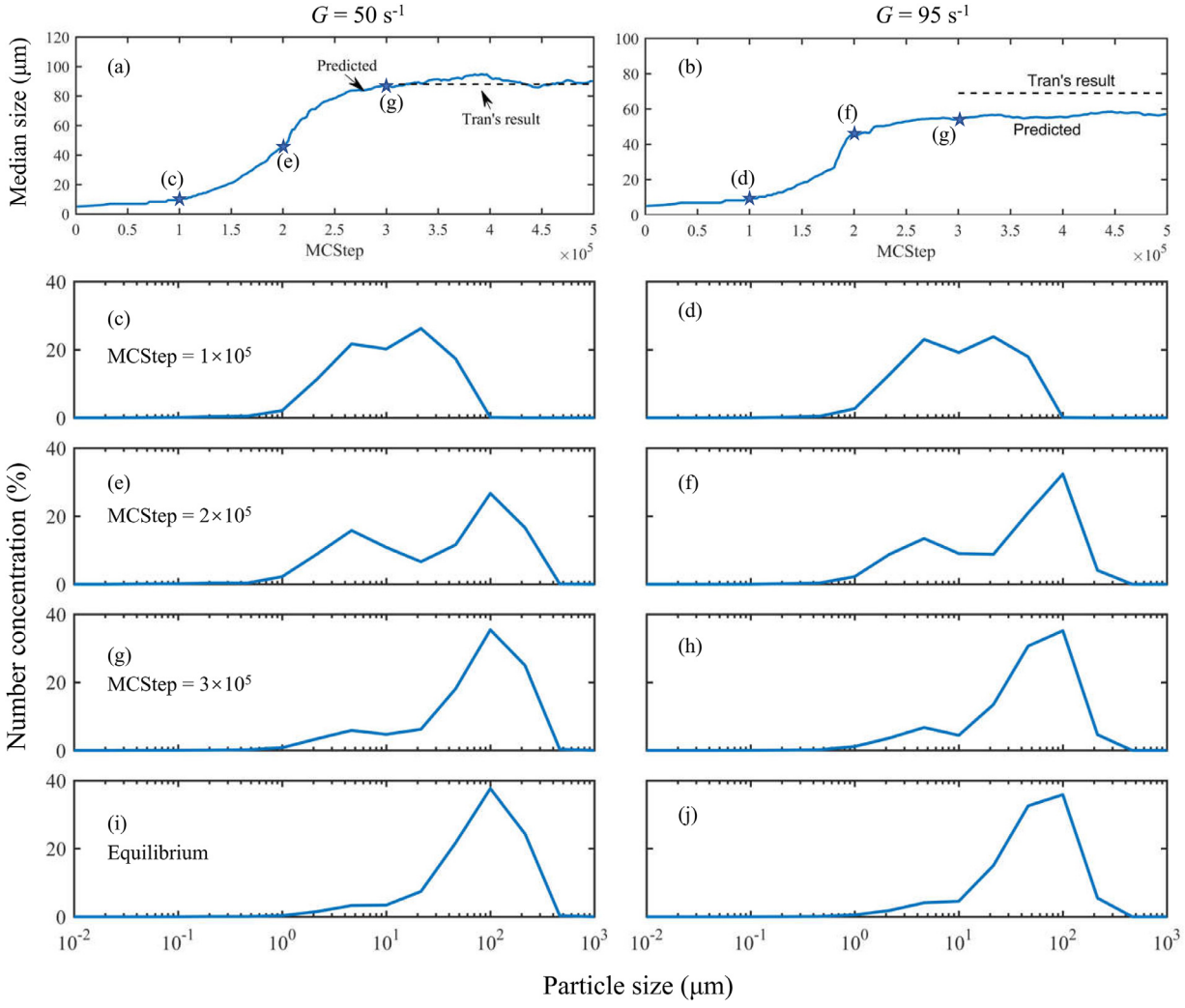

Fig. 6. The predicted and experimental characteristic sizes and the predicted FSDs for turbulent shear rate $G=50$ s^{-1} (the first column) and $G=95$ s^{-1} (the second column) respectively.

It can be observed in Fig. 6 (a) and (b) that the aggregation dominates in the first 2×10^5 MC steps. But the particle size grows at a low speed within the first 10^5 MC steps since the floc size still remains in the small level. The rate of increasing of floc size is higher between 1×10^5 and 2×10^5 MC steps and larger flocs start to appear. After 2×10^5 MC steps, the fragmentation rate gradually rises and the slope of the curve of median floc size is getting flatter. The system approaches an equilibrium state at 3×10^5 MC steps, around which the aggregation and fragmentation are closely matched in rate and the characteristic size keeps fluctuating. In order to eliminate the error from the fluctuation, the equilibrium result is calculated by averaging the results of the last 2×10^5 MC steps. The fractal dimension ($nf=2.2$) was calibrated under the shear condition $G=50$ s^{-1}, and the results for high shear condition were treated as validation cases. The predicted D_{50} when the turbulent shear $G=50$ s^{-1} is 90.02 μm, which is highly consistent with the experiment result 88 μm. When it comes to higher turbulent shear condition, the simulated median size is 56.7 μm and appears to be slightly underestimated compared with the experimental result of 69 μm. The bias for the low shear condition ($G=50$ s^{-1}) was mainly statistical noise caused by sampling, which is inherent to any QMC approach. This error can be reduced with sufficient simulation particles (Hao et al., 2013). For the high shear condition ($G=95$ s^{-1}) the error of median size was 17.8 %. This error seems reasonable as a model system error, as higher values (up to 27.2%) have been reported by Mietta et al. (2008). A possible reason accounted for this underestimation is that the fragmentation frequency assumption or/and the aggregation efficiency

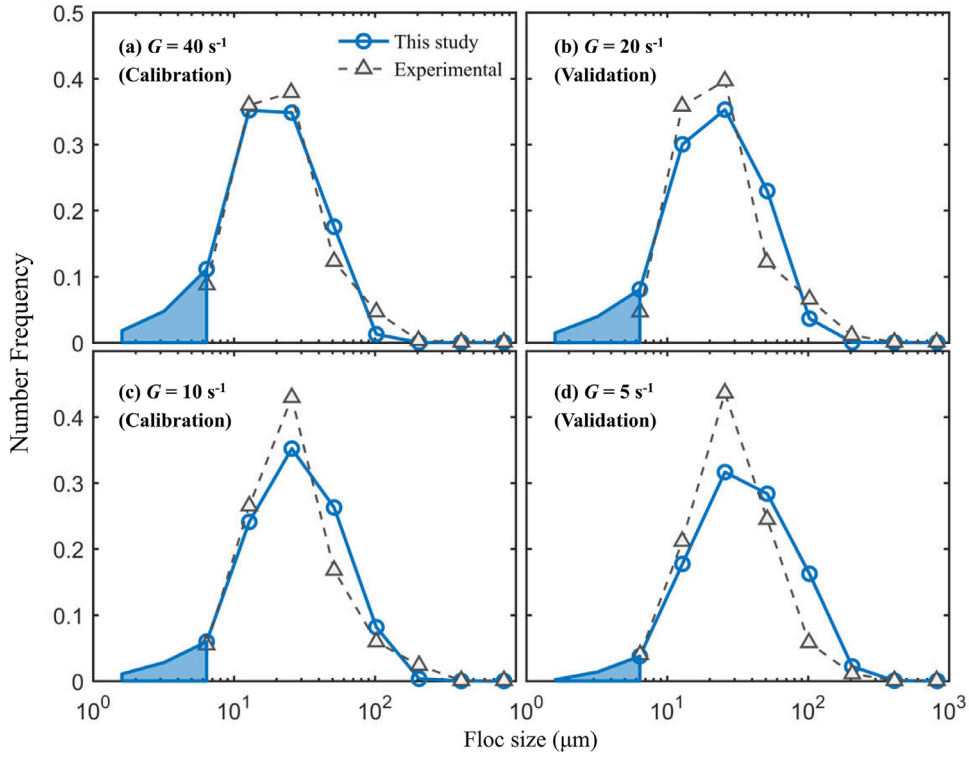

Fig. 7. Comparison between predicted and experimental FSDs of equilibrium for (a) (c) calibration and (b) (d) validation results for suspended kaolinite with different turbulent shear rate.

assumption or/and the fractal dimension are insufficient in a high-intensity turbulent field. It is also critical to note that fixing the fractal dimension cannot account for this error. The change of fractal dimension from the constant 2.2 to a variable term (with δ calibrated using Eq. 6) would not help improving the accuracy in this case. With the calibrated value δ = -0.046, the error of the median size under $G = 95\ s^{-1}$ went up to 21.1%. In addition, one can directly obtain the predicted FSD by the MC model at any time step. The predicted FSD at MC Step = 1×10^5, 2×10^5, 3×10^5, and the equilibrium state are given in Fig. 6.

Case V: Maggi's settling column experiment

Maggi et al. (2002, 2007) carried out a numerical study to explore the effect of variable fractal dimension on the FSD in a laboratory settling column with suspended kaolinite. The settling column is about 480 cm high with an inside diameter of 30 cm, above which a buffer tank is set to continuously mix and dilute the highly-concentrated suspension to the test concentration. The homogeneous turbulence field is produced by an oscillating 3-D grid to induce flocculation. Flocs settle through the turbulent field and are recorded by the camera system in the measuring section under the settling column. The experiment is performed with four turbulent shear rates G = 5, 10, 20, and 40 s^{-1} respectively and a constant sediment concentration of c = 500 mg/L. The density of the selected kaolinite is $\rho_s \approx 2650\ kg/m^3$ and its mineral size is in the range 0.1 – 5 μm. The observation window is 6-by-6 mm^2 and the resolution is 6.42 μm/pixel, which limits the scope of measurement, and overestimates the number concentration.

The experimental FSDs for G = 10 and 40 s^{-1} are used to calibrate the fitting parameters such as fractal dimension and fragmentation function. The other two shear rates are used to validate the model results. The fitting parameters are given in Table. 1. The initial particle distribution obeys a Gaussian distribution like case IV except that the D_p in this case is 2 μm. The maximum floc size is selected as the Kolmogorov scale, and the fractal dimension is set variable with the coefficient $\delta = -0.1$ recommended in Maggi et al. (2005, 2007, 2008).

The predicted and experimental results of the FSD at equilibrium state are given in Fig. 7. Note that the size classes under 6.4 μm are shown either in the FSDs in the blue shadow areas with solid edges to demonstrate the level of detail this study can provide. The FSDs given by the other solid lines are calculated by normalization of particle arrays excluding the particle smaller than 6.4 μm, and the size classes are the same as those in Maggi et al. (2007). As can be seen in Fig. 7, the predicted FSDs of the four turbulent shear rates match quite well with the experimental results.

One can see that for the case of the lower turbulent shear rate G = 5 s^{-1}, the simulated FSD seems to slightly overestimate the fraction of large particles. It might be a consequence of the underestimation of A_{max} in Eq. 10 for low shear rates. The term of turbulent shear is smaller when the shear rate is lower, so the differential settling term is more dominant in the calculation of aggregation kernel and the A_{max} would be underestimated under the simplification that differential settling is zero. This leads to an overestimation of the aggregation rate of small particles. Another possible reason is that the assumption of aggregation efficiency or/and breakup function or/and binary fragmentation are less appropriate for kaolinite flocculation. Further study and improvement will be needed to accord for it.

The predicted and experimental median size (D_{50}) is shown in Fig. 8. Note that the median size of the experimental result is calculated by FSDs using linear interpolation. The predicted and experimental results match in good accuracy. The predicted median size is getting smaller as compared to the predicted result with increasing turbulent shear rate. Several reasons may be accounted for this trend. Firstly, particles smaller than 6.4 μm are neglected in the experimental results due to the resolution of the camera system, which would introduce a bias towards larger sizes in measurement. Secondly, the selection of D_{max} or/and the assumptions

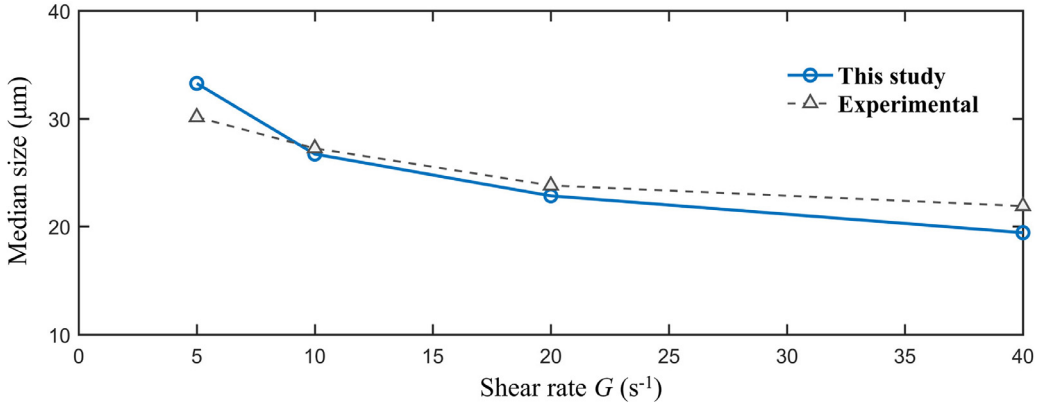

Fig. 8. Comparison between predicted and experimental characteristic sizes of equilibrium for suspended kaolinite with different turbulent shear rate.

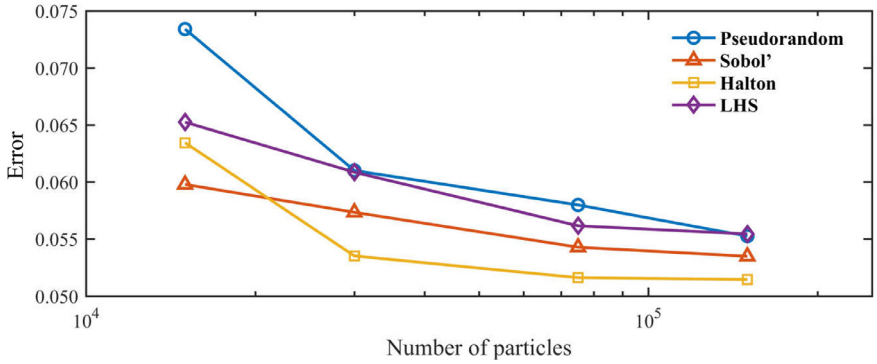

Fig. 9. The errors between predicted and experimental results using different QMC sampling schemes for different number of particles.

about aggregation efficiency and fragmentation are insufficient to represent kaolinite flocculation.

4. Discussion

4.1. Monte Carlo and Quasi-Monte Carlo sampling

In this section, a numerical example, combining aggregation and fragmentation where an exact analytical solution is known (case V in section 3), is used to compare the accuracy and efficiency of different QMC methods and the LHS scheme described above with the standard MC scheme. MC simulations run in a PC equipped with a CPU of Intel(R) Core(TM) i7-9750H CPU @2.60GHz and memory of 16 GB. The error that describes how well the FSD approximates the analytical solution is defined as

$$E_r = \sum_{i=1}^{N_c} \left| n_i(D,t) - n_i^A(D,t) \right| \tag{30}$$

where $N_C = 10$ is the number of size classes, the superscript A indicates the analytical solution. The simulations were conducted with different numbers of particles $N = 15{,}000$, 30,000, 75,000, and 150,000, and the MC steps were set to 5×10^5, 5×10^5, 7×10^5, and 15×10^5 respectively to make sure that equilibrium is reached.

The FSDs results of all the schemes converge towards the analytical solution as N increases (Fig. 9). Note that the errors of all schemes decrease significantly when N is larger than 30,000, and the benefit (reduction of error) decreases with further increase of N. In addition, errors of two QMC methods and the LHS scheme are always smaller than standard MC methods using pseudorandom numbers (also see Table 1). The result simulated using the Halton sequence reaches the highest accuracy when N is larger than 30,000. In other words, compared to the other three schemes, the QMC scheme using Halton sequence requires the least particle numbers in simulated system to reach reasonable accuracy ($E_r < 0.055$ in this case).

The computational costs of the four different MC methods are also tested (Fig. 10). Since the producing algorithm of quasi-numbers induces extra cost or/and the codes might not be optimized yet, the time consumptions of pre-producing random number series are not included. In addition, the time consumption of simulation with LHS sequence is not tested due to its low efficiency of pre-production. The required CPU time of QMC schemes using Sobol' and Halton sequences with any number of particles N are less than the standard MC method (Fig. 10 and Table 2). The simulation using Halton sequence saved more CPU time compared to that by using other two random number series when N is larger than 30,000. Note that the CPU time reduction of QMC compared to standard MC is around 8% with particle numbers $N = 1.5\times10^5$. It is reasonable to expect that the QMC method would save more calculation cost in solving the high dimensional problem (e.g. bio-adhesion included PBM).

4.2. Sensitivity tests

(1) Breakage events

The fragmentation distribution function plays an important role in predicting the steady-state FSD and characteristic sizes (Maggi, 2005; Khelifa and Hill, 2006; Shin et al., 2015). However, there were only simple theoretical assumptions about the fragmentation distribution since it is still difficult to carry out laboratory experiment to observe the micro-scale fragmentation processes directly (Maggi, 2005; Spicer and Pratsinis, 1996). In order to explore the influence of different fragmentation distribution functions on the modeling results, the three simplest assumptions, including binary breakup with mass ratio 1:1 (Eq. 12), ternary breakup with

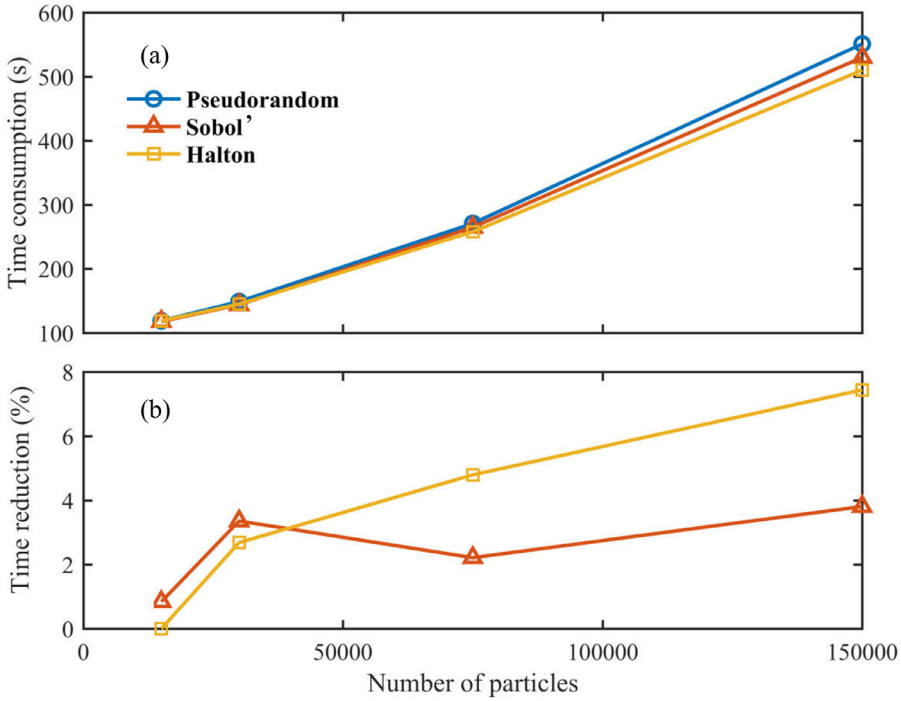

Fig. 10. The time consumptions of simulation using different QMC sampling schemes for different number of particles. (a) Absolute time consumption; (b) time reductions compare to pseudorandom sequence (standard MC).

Table. 2
The errors and the time consumptions of different RNG functions with $N = 15000$, 30000, 75000, and 150000.

	$N = 15000$	$N = 30000$	$N = 75000$	$N = 150000$
ERROR				
Pseudorandom	0.07341	0.06100	0.05799	0.05525
Sobol'	0.05979	0.05735	0.05428	0.05348
Halton	0.06345	0.05351	0.05162	0.05146
LHS	0.06525	0.06085	0.05616	0.05544
TIME CONSUMPTION (s)[a]				
Pseudorandom	119	149	271	551
Sobol	118	144	265	530
Halton	119	145	258	510

[a] The time consumption of simulation using LHS sequence is not included due to its low efficiency of pretreatments.

mass ratio 1:1:2 (Eq. 31), and uniform breakup (Eq. 24~25) (e.g., Spicer and Pratsinis, 1996; Shen and Maa, 2015,2016), are tested in the model and compared to the experimental data with different turbulent shear rates by Maggi et al. (2007).

$$\begin{cases} N_{fi'} = r_4 N_{fi} \\ N_{fi''} = N_{fi'''} = (1 - r_4) N_{fi}/2 \end{cases} \quad (31)$$

The results given in Fig. 11 show that different fragmentation distribution functions will lead to significantly different predictions. Compared to the binary breakup assumption, the predicted FSDs from the ternary and the uniform breakup assumptions are skewed towards smaller size classes. The predicted median sizes simulated by using binary breakup function are higher than those by the other two assumptions. The results of the median sizes show a tendency that more fragments are produced after each fragmentation event, which will result in lower median sizes. This is to be expected since the mean size of fragments is smaller than that with assumptions of less fragments.

It seems that using the binary fragmentation gives a much better match of both FSDs and median sizes. This assumption seems reasonable since Kramer and Clark (1999) proposed that the probability for a floc breaking into multiple fragments is small, and Tsai and Hwang (1995) found that flocs are prone to binary breakup into fragments with similar size. From another perspective, breakage into multiple fragments, which occurs infrequently, can be seen as several simultaneous binary fragmentation events. Nevertheless, selection of the breakage distribution function still requires a better understanding of floc structure (e.g., fractal property, density) and the breakup process under hydrodynamic impact.

(2) Effects of fractal dimension

The fractal dimension *nf* is used to empirically relate the geometry of flocs to their density, strength and settling velocity. Usually, *nf* is estimated from experimental floc size and settling velocity data. Note that the fractal dimension of flocs with even the same size may be different since flocs might not be self-similar at all, which is the basic assumption in the definition of fractal dimension. Most studies usually assume a constant *nf* on empirical understanding (Winterwerp, 1998), or an exponent form *nf* based on the knowledge that large particles have low *nf* than smaller particles (Khelifa and Hill, 2006; Maggi et al., 2007). Son and Hsu (2008) found that a change of fractal dimension (from a constant to a power law) does not obviously improve the estimation of steady-state median size. Khelifa and Hill (2006) proposed an

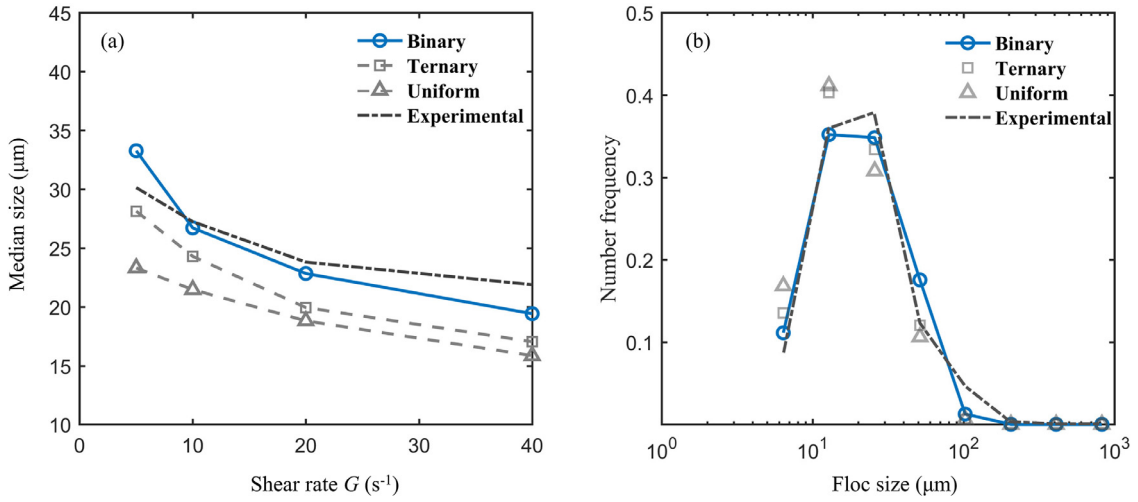

Fig. 11. Sensitivity tests for different fragmentation distribution functions in simulation for their (a) characteristic sizes and (b) FSDs.

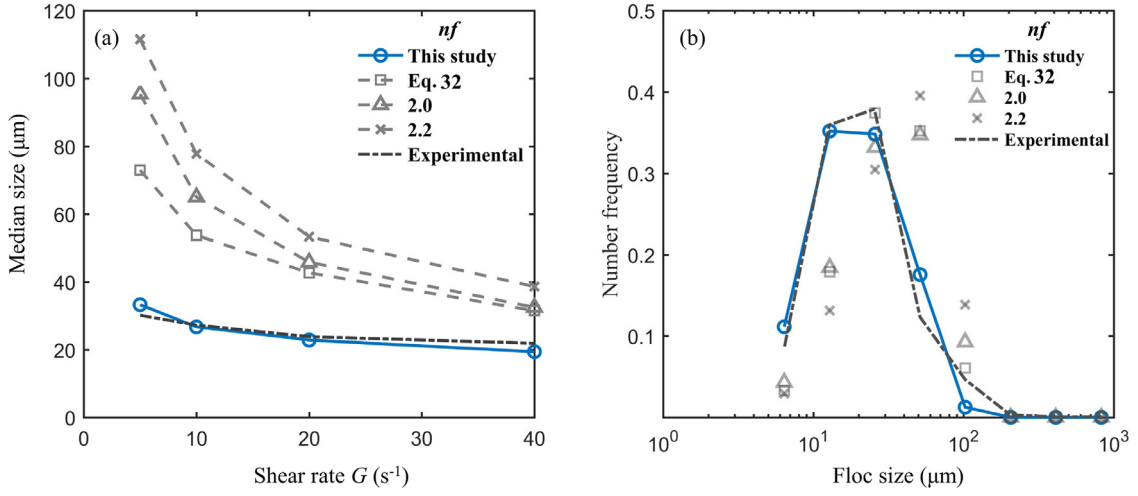

Fig. 12. Sensitivity tests for different constant and variable fractal dimensions in simulation for their (a) characteristic sizes and (b) FSDs.

estimation of the coefficient δ in Eq. 1:

$$\delta = \frac{\log(F_c/3)}{log\left(D_{fc}/D_p\right)} \tag{32}$$

where $D_{fc} = 2{,}000$ μm and $F_c = 2$ are suggested in Khelifa and Hill (2006).

As is shown in Fig. 12, the predicted FSDs at steady state are quite sensitive to the fractal dimension *nf*. Using the constant $nf = 2.2$, both the modelling FSD skews toward the larger classes and the median size is larger than that by using the constant $nf = 2.0$. This is expected since flocs with a higher fractal dimension are more solid than those with a low fractal dimension. Another reason may be that the differential settling term in Eq. 2 becomes more important relative to the turbulent shear term since the velocity differences between small flocs and big flocs are significant compared to the case of low *nf*. Results from using a variable *nf* show a higher accuracy with experimental data. The value of coefficient $\delta = -0.1$ suggested by Maggi et al. (2005, 2007, 2008) matched quite well both the FSDs and the median sizes.

However, it is worth to mention that the predicted median sizes using constant *nf* and variable *nf* by Eq. 32 decrease rapidly with the turbulent shear increasing. In other words, the relative errors of D_{50} of those three cases using different *nf* reduced to nearly 30% when the turbulent shear rate is high. It might indicate that the calculation of differential settling (Eq. 4) is overestimated when the turbulent shear rate is low. In addition, the maximum aggregation kernel $A_{\max}$ calculated by Eq. 5 neglects the effect of differential settling, which may cause an error when the turbulent shear rate is low to some extent.

It is widely accepted that the density of the flocs decrease as a function of floc size. To better investigate their relationship, the variations of the excess density of the flocs were also simulated.

$$\Delta\rho_f \propto (\rho_s - \rho_w)\left[\frac{D_p}{D_f}\right]^{3-nf} \tag{33}$$

where $\rho_w = 1000$ kg/m^3 is the density of water. Under the turbulent shear rate $G = 40$ s^{-1}, it can be seen that the floc size increases while the floc density deceases with QMC steps, which indicates that the density of the flocs often decrease as a function of floc size (Fig. 13).

4.3. Connections with field-scale sediment models

With the rapid growth of computational ability, a large quantity of field-scale numerical models for simulating hydrodynamics and sediment transport have been developed in recent decades. According to the consideration of computational spatial dimension, these numerical models can be classified as one-dimensional models (e.g., MOBED and FLUVIAL 11), 2-dimensional models

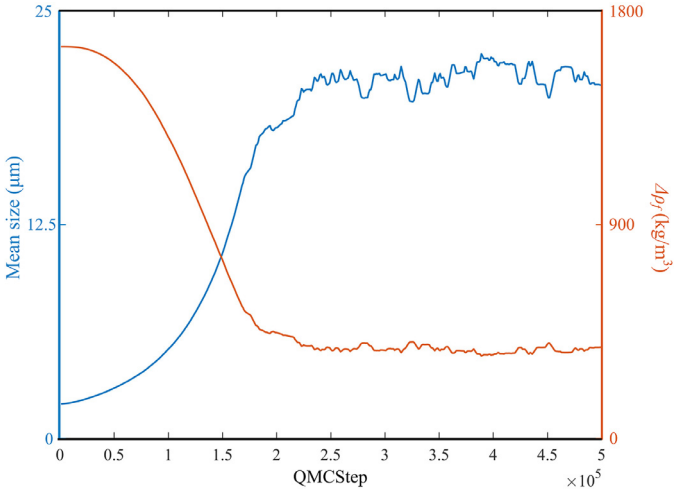

Fig. 13. The change of the mean size and the excess density of flocs with QMC steps.

(e.g., SERATRA, Delft 2D and MIKE 21), and 3-dimensional models (e.g., TELEMAC, Delft 3D, and ROMS) (Krishnappan, 1981; Chang, 1984; Onishi and Wise, 1982; Walstra et al., 1998; Warren and Bach, 1992; Hervouet and Bates, 2000; Delft Hydraulic, 1999; Song and Haidvogel, 1994). One of the most important parameters in simulating sediment transport and estuarine and coastal evolution is the settling velocity (*ws*) of cohesive sediments, which is controlled by floc size, floc shape, and floc density. However, the settling velocity is often treated as an arbitrary (although reasonable) constant or a fitting parameter in most field-scale models. However, it usually does not match the measured *ws* (Papanicolaou et al, 2008; Toorman, 2012; Horemans et al., 2020). The lack of understanding of flocculation mechanisms would cause biased estimations in large-scale simulation for sediment transport processes.

Numerical models focused on multi-class cohesive sediment flocculation often give a better estimation of the settling flux but consume more computing resources with an increasing number of size classes (Lee et al, 2011; Toorman, 2012; Zhang et al., 2013; Shen and Maa, 2017). The PBM framework contains external and internal variables: the former describe the physical space of the location of particles, and the latter account for one or several distinguishable properties of particles such as size, volume, and biomass fraction (Shen and Maa, 2016; Iveson, 2002). The computational resources of PBM increase rapidly with the inclusion of additional internal variables. Thus, the PBM accounting for size in any 3-D model (i.e., with three external variables *x, y*, and *z*) is actually a 4-D model, which demands expensive computational costs and thus has not been widely adopted consequently. Nevertheless, simplified PBMs, e.g., the two-class PBM (Lee et al., 2011) and the three-class PBM (Shen et al., 2018a, 2018b), have already been employed in cohesive sediment studies. There is still a broad space for multiple class PBMs to be investigated in cohesive sediment field.

It is also crucial to note that methods such as the simplified Lagrangian model (Winterwerp, 1998) and the PBM solved by the discretization method (e.g., Krishnappan and Marsalek, 2002; Liu et al., 2019; Verney et al., 2011) or the quadrature method of moments (e.g., Shen and Maa, 2015, 2016; Li et al., 2019) have explicit mathematical formulae. They are in favor of being coupled into hydrodynamic models to simulate cohesive sediment transport process. For instance, Krishnappan and Marsalek (2002) proposed a coupled 1-D advection-diffusion and pure-aggregation PBM to predict the sediment flocs from an on-stream stormwater management pond, and Liu et al. (2019) implemented the PBM in a large eddy simulation of wave-driven Langmuir turbulence. On the other hand, the QMC models cannot be directly coupled with field-scale model in estuarine and coastal waters at current stage. Regarding the application of stochastic methods in modeling the flocculation process, most of the existing works are based on the Winterwerp's formula. For example, Maggi (2008) proposed a stochastic Lagrangian model to explore the temporal variability of the median floc size, similar as shown in Fig. 6(a)(b), and Shin et al. (2015) adopted a MC method to determine the breakup probability and could calculate the FSD in log-normal forms. Nevertheless, their models seem difficult to extend to account for flocculation of bio-mineral aggregates with multi-modal FSDs due to the uncertainty and complexity of biomass-sediment interaction (Shen et al., 2019).

The QMC models produce a new stochastic way to solve PBM and help determining various micro-scale flocculation behaviors, which provides new prospects to improve low cost bio-flocculation models to couple with large-scale model. Possibly coupled with computational fluid dynamics (CFD) in turbulent flow (Liu and Chan, 2017; Xu et al., 2017), the QMC based PBMs also have the potential to simulate the interactions between turbulence and flocculated particles in the future.

5. Conclusions

The following conclusions can be drawn for this study:

(1) The quasi-Monte Carlo method is applied to develop a flocculation model by a size-based population balance model for cohesive sediments. The maximum relative errors of the mean sizes are less than 10%.
(2) The settling column experimental results for suspended kaolinite with a concentration of 500 mg/L and different shear rates carried out by Maggi et al. (2002) are used to validate the simulated FSD and its median size. The QMC model predicted these well by selecting similar coefficients in aggregation and fragmentation processes given by Mietta et al. (2008). The results of simulated median size for a laboratory experiment conducted by Tran and Strom (2017) also show a reasonable agreement.
(3) The calculation accuracies and time consumptions of different QMC schemes and the LHS scheme were tested. All three considered low-discrepancy number schemes show better accuracy than the standard MC method, among which the QMC scheme using the Halton sequence is the best one in accuracy. On the other side, compared to the other schemes, the QMC scheme with Halton sequence requires the least particle numbers in simulated system to reach a reasonable accuracy. The CPU time of schemes using the Halton sequence and the Sobol' sequence are less than that of standard MC. In this case, one can save around 8% CPU time with $N = 1.5\times10^5$ by replacing the pseudo-random number by the Halton sequence.
(4) The model prediction will be significantly influenced by assumptions on the fractal dimension nf and fragmentation distribution functions, which should be checked carefully in every model for different applications.
(5) The reasonable performance of the QMC model for cohesive sediments shows great prospect in solving multivariate and high dimensional problem (e.g. biomass effect on flocculation) due to its nature of discretion.

Declaration of Competing Interest

The authors declare that they have no known competing financial interests or personal relationships that could have appeared to influence the work reported in this paper.

Acknowledgments

The authors would like to acknowledge the funding support from the National Natural Science Foundation of China (Grant No. U2040203 & 51909068 & 52011540388), the Fundamental Research Funds for the Central Universities of China (Grant No. B200201009), the Research Funds of Shanghai Municipal Water Authority (Grant No. 2020-02), the Open Funds of the Key Laboratory of Ministry of Education for Coastal Disaster and Protection of China (Grant No. 201901 & 202004), and the Open Funds of State Key Laboratory of Hydraulic Engineering Simulation and Safety of China (Grant No. HESS-1917). This study was also supported under the framework of international cooperation program managed by the National Research Foundation of Korea (2020K2A9A2A06036472, FY2020).

References

Azhikodan, G., Yokoyama, K., 2021. Erosion and sedimentation pattern of fine sediments and its physical characteristics in a macrotidal estuary. Science of The Total Environment 753, 142025, . doi:10.1016/j.scitotenv.2020.142025.

Bertin, D., Cotabarren, I., Piña, J., Bucalá, V., 2016. Population balance discretization for growth, attrition, aggregation, breakage and nucleation. Computers & Chemical Engineering 84, 132–150. doi:10.1016/j.compchemeng.2015.08.011.

Burchard, H., Schuttelaars, H.M., Ralston, D.K., 2018. Sediment Trapping in Estuaries. Annual Review of Marine Science 10, 371–395. doi:10.1146/annurev-marine-010816-060535.

Burhenne, S., Jacob, D., Henze, G.P., 2011. Sampling based on Sobol' sequences for Monte Carlo techniques applied to building simulations. In: Proceedings of Building Simulation 2011: 12th Conference of International Building Performance Simulation Association, Sydney, Australia, pp. 1816–1823 14-16 November 2011.

Caflisch, R.E., 1998. Monte carlo and quasi-monte carlo methods. Acta Numerica 7, 1–49. doi:10.1017/S0962492900002804.

Chang, H.H, 1984. Modeling of river channel changes. Journal of Hydraulic Engineering 110 (2), 157–172. doi:10.1061/(ASCE)0733-9429(1984)110:2(157).

Chi, H., Mascagni, M., Warnock, T., 2005. On the optimal Halton sequence. Mathematics and Computers in Simulation 70 (1), 9–21. doi:10.1016/j.matcom.2005.03.004.

Das, A., Bück, A., Kumar, J., 2020. Selection function in breakage processes: PBM and Monte Carlo modeling. Advanced Powder Technology 31 (4), 1457–1469. doi:10.1016/j.apt.2020.01.002.

Dick, J., Kuo, F.Y., Sloan, I.H., 2013. High-dimensional integration: The quasi-Monte Carlo way. Acta Numerica 22, 133–288. doi:10.1017/S0962492913000044.

Edmonds, D.A., Slingerland, R.L., 2010. Significant effect of sediment cohesion on delta morphology. Nature Geoscience 3 (2), 105–109. doi:10.1038/ngeo730.

Eibeck, A., Wagner, W., 2001. Stochastic particle approximations for Smoluchoski's coagulation equation. Annals of Applied Probability 11, 1137–1165. doi:10.2307/2699912.

Fall, K.A., Friedrichs, C.T., Massey, G.M., Bowers, D.G., Smith, S.J., 2021. The importance of organic content to fractal floc properties in estuarine surface waters: Insights from video, LISST, and pump sampling. Journal of Geophysical Research: Oceans doi:10.1029/2020JC016787, 2020JC016787.

Garcia, A.L., Van Den Broeck, C., Aertsens, M., Serneels, R., 1987. A Monte Carlo simulation of coagulation. Physica A: Statistical Mechanics and its Applications 143 (3), 535–546. doi:10.1016/0378-4371(87)90164-6.

Geyer, W.R., MacCready, P., 2014. The Estuarine Circulation. Annual Review of Fluid Mechanics 46, 175–197. doi:10.1146/annurev-fluid-010313-141302.

Halton, J.H., 1960. On the efficiency of certain quasi-random sequences of points in evaluating multi-dimensional integrals. Numerische Mathematik 2 (1), 84–90.

Hao, X., Zhao, H., Xu, Z., Zheng, C., 2013. Population balance-Monte Carlo simulation for gas-to-particle synthesis of nanoparticles. Aerosol science and technology 47 (10), 1125–1133. doi:10.1080/02786826.2013.823642.

Hervouet, J.M., Bates, P., 2000. The TELEMAC modelling system. Hydrological Processes 14 (13).

Hess, S., Polak, J., 2003. An alternative method to the scrambled Halton sequence for removing correlation between standard Halton sequences in high dimensions. 43rd Congress of the European Regional Science Association: "Peripheries, Centres, and Spatial Development in the New Europe August 2003, http://hdl.handle.net/10419/116163 .

Horemans, D.M.L., Dijkstra, Y.M., Schuttelaars, H.M., Meire, P., Cox, T.J.S., 2020. Unraveling the Essential Effects of Flocculation on Large-Scale Sediment Transport Patterns in a Tide-Dominated Estuary. Journal of Physical Oceanography 50 (7), 1957–1981. doi:10.1175/JPO-D-19-0232.1.

Hou, T., Nuyens, D., Roels, S., Janssen, H., 2019. Quasi-Monte Carlo based uncertainty analysis: Sampling efficiency and error estimation in engineering applications. Reliability Engineering & System Safety 191, 106549, . doi:10.1016/j.ress.2019.106549.

Hydraulics, D., 1999. Delft3D users' manual. Delft Hydraulics, The Netherlands.

Iveson, S.M., 2002. Limitations of one-dimensional population balance models of wet granulation processes. Powder Technology 124 (3), 219–229. doi:10.1016/S0032-5910(02)00026-8.

Kariwala, V., Cao, Y., Nagy, K., Z., 2012. Automatic differentiation-based quadrature method of moments for solving population balance equations. AIChE Journal 58 (3), 842–854. doi:10.1002/aic.12613.

Keramat, M., Kielbasa, R., 1997. Latin hypercube sampling Monte Carlo estimation of average quality index for integrated circuits. Analog Integrated Circuits and Signal Processing 14 (1-2), 131–142.

Keyvani, A., Strom, K., 2014. Influence of cycles of high and low turbulent shear on the growth rate and equilibrium size of mud flocs. Marine Geology 354, 1–14. doi:10.1016/j.margeo.2014.04.010.

Khelifa, A., Hill, P., 2006. Kinematic assessment of floc formation using a Monte Carlo model. Journal of Hydraulic Research 44 (4), 548–559. doi:10.1080/00221686.2006.9521705.

Khelifa, A., Hill, P.S., Lee, K., 2005. Assessment of minimum sediment concentration for OMA formation using a Monte Carlo model. In: Al-Azab, M., El-Shorbagy, W. (Eds.), Developments in Earth and Environmental Sciences. Elsevier, pp. 93–104. doi:10.1016/S1571-9197(05)80031-X.

Kiørboe, T., Andersen, K.P., Dam, H.G., 1990. Coagulation efficiency and aggregate formation in marine phytoplankton. Marine Biology 107 (2), 235–245. doi:10.1007/BF01319822.

Kotalczyk, G., Kruis, F.E., 2017. A Monte Carlo method for the simulation of coagulation and nucleation based on weighted particles and the concepts of stochastic resolution and merging. Journal of Computational Physics 340, 276–296. doi:10.1016/j.jcp.2017.03.041.

Kramer, T.A., Clark, M.M., 1999. Incorporation of aggregate breakup in the simulation of orthokinetic coagulation. Journal of colloid and interface science 216 (1), 116–126. doi:10.1006/jcis.1999.6305.

Krishnappan, B.G, 1981. User's manual: Unsteady, non-uniform, mobile boundary flow model—MOBED. *Hydraulic Division*. National Water Research Institute, CCIW, Burlington, Ontario.

Krishnappan, B.G., Marsalek, J., 2002. Modelling of flocculation and transport of cohesive sediment from an on-stream stormwater detention pond. Water Research 36 (15), 3849–3859. doi:10.1016/S0043-1354(02)00087-8.

Kruis, F.E., Maisels, A., Fissan, H., 2000. Direct simulation Monte Carlo method for particle coagulation and aggregation. AIChE Journal 46 (9), 1735–1742. doi:10.1002/aic.690460905.

Kumar, S., Ramkrishna, D., 1996. On the solution of population balance equations by discretization—I. A fixed pivot technique. Chemical Engineering Science 51 (8), 1311–1332. doi:10.1016/0009-2509(96)88489-2.

Kumar, J., Kaur, G., Tsotsas, E., 2016. An accurate and efficient discrete formulation of aggregation population balance equation. Kinetic & Related Models 9 (2), 373. doi:10.3934/krm.2016.9.373.

Kuprenas, R., Tran, D., Strom, K., 2018. A shear-limited flocculation model for dynamically predicting average floc size. Journal of Geophysical Research: Oceans 123 (9), 6736–6752. doi:10.1029/2018JC014154.

Lai, H., Fang, H., Huang, L., He, G., Reible, D., 2018. A review on sediment bioflocculation: Dynamics, influencing factors and modeling. Science of the total environment 642, 1184–1200. doi:10.1016/j.scitotenv.2018.06.101.

Lee, B.J., Toorman, E., Molz, F.J., Wang, J., 2011. A two-class population balance equation yielding bimodal flocculation of marine or estuarine sediments. Water Research 45 (5), 2131–2145. doi:10.1016/j.watres.2010.12.028.

Lee, B.J., Molz, F., 2014. Numerical simulation of turbulence-induced flocculation and sedimentation in a flocculant-aided sediment retention pond. Environmental Engineering Research 19 (2), 165–174. doi:10.4491/eer.2014.19.2.165.

Lee, K.F., Patterson, R.I.A., Wagner, W., Kraft, M., 2015. Stochastic weighted particle methods for population balance equations with coagulation, fragmentation and spatial inhomogeneity. Journal of Computational Physics 303, 1–18. doi:10.1016/j.jcp.2015.09.031.

Li, D., Li, Z., Gao, Z., 2019. Quadrature-based moment methods for the population balance equation: An algorithm review. Chinese Journal of Chemical Engineering 27 (3), 483–500. doi:10.1016/j.cjche.2018.11.028.

Liffman, K., 1992. A Direct Simulation Monte Carlo Method for Cluster Coagulation. Journal of Computational Physics 100 (1), 116–127. doi:10.1016/0021-9991(92)90314-O.

Lin, Y., Lee, K., Matsoukas, T., 2002. Solution of the population balance equation using constant-number Monte Carlo. Chemical Engineering Science 57 (12), 2241–2252. doi:10.1016/S0009-2509(02)00114-8.

Liu, J., Liang, J.H., Xu, K., Chen, Q., Ozdemir, C.E., 2019. Modeling sediment flocculation in Langmuir turbulence. Journal of Geophysical Research: Oceans 124 (11), 7883–7907. doi:10.1029/2019JC015197.

Liu, S., Chan, T.L., 2017. A coupled CFD-Monte Carlo method for simulating complex aerosol dynamics in turbulent flows. Aerosol Science and Technology 51 (3), 269–281. doi:10.1080/02786826.2016.1260087.

Maggi, F., 2005. Flocculation dynamics of cohesive sediment. Delft University of Technology, Netherlands Ph.D. Dissertation.

Maggi, F., 2008. Stochastic flocculation of cohesive sediment: analysis of floc mobility within the floc size spectrum. Water Resources Research 44 (1). doi:10.1029/2007WR006109.

Maggi, F., Mietta, F., Winterwerp, J.C., 2007. Effect of variable fractal dimension on the floc size distribution of suspended cohesive sediment. Journal of Hydrology 343 (1-2), 43–55. doi:10.1016/j.jhydrol.2007.05.035.
Maggi, F., Winterwerp, J., Fontijn, H., van Kesteren, W., Cornelisse, J., 2002. A settling column for turbulence-induced flocculation of cohesive sediments, in: Tony L. Wahl, Clifford A. Pugh, Kevin A. Oberg, and Tracy B. Vermeyen (Eds.), Hydraulic Measurements and Experimental Methods 2002, pp. 1-10.
Marchisio, D.L., Pikturna, J.T., Fox, R.O., Vigil, R.D., Barresi, A.A., 2003a. Quadrature method of moments for population-balance equations. AIChE Journal 49 (5), 1266–1276. doi:10.1002/aic.690490517.
Marchisio, D.L., Vigil, R.D., Fox, R.O., 2003b. Quadrature method of moments for aggregation–breakage processes. Journal of Colloid and Interface Science 258 (2), 322–334. doi:10.1016/S0021-9797(02)00054-1.
Mascagni, M., Chi, H., 2004. On the scrambled halton sequence. Monte Carlo Methods and Applications 10 (3-4), 435–442. doi:10.1515/mcma.2004.10.3-4.435.
McCave, I., 1984. Size spectra and aggregation of suspended particles in the deep ocean. Deep Sea Research Part A. Deep Sea Research Part A. Oceanographic Research Papers 31 (4), 329–352. doi:10.1016/0198-0149(84)90088-8.
McCoy, B.J., Madras, G., 2003. Analytical solution for a population balance equation with aggregation and fragmentation. Chemical Engineering Science 58 (13), 3049–3051. doi:10.1016/S0009-2509(03)00159-3.
McGraw, R., 1997. Description of aerosol dynamics by the quadrature method of moments. Aerosol Science and Technology 27 (2), 255–265. doi:10.1080/02786829708965471.
McKay, M., Beckman, R., 1979. A comparison of three methods for selecting values of input variables in the analysis of output from a computer code. Technometrics 21 (2). doi:10.1080/00401706.1979.10489755.
Mietta, F., Maggi, F., Winterwerp, J.C., 2008. Chapter 19 Sensitivity to breakup functions of a population balance equation for cohesive sediments. INTERCOH 2005. Sediment and Ecohydraulics 9, 275–286. doi:10.1016/S1568-2692(08)80021-6.
Mietta, F., Chassagne, C., Verney, R., Winterwerp, J.C., 2011. On the behavior of mud floc size distribution: model calibration and model behavior. Ocean Dynamics 61 (2-3), 257–271. doi:10.1007/s10236-010-0330-2.
Olsson, A., Sandberg, G., Dahlblom, O., 2003. On Latin hypercube sampling for structural reliability analysis. Structural safety 25 (1), 47–68. doi:10.1016/S0167-4730(02)00039-5.
Olsson, A.M., Sandberg, G.E., 2002. Latin hypercube sampling for stochastic finite element analysis. Journal of Engineering Mechanics 128 (1), 121–125. doi:10.1061/(ASCE)0733-9399(2002)128:1(121).
Onishi, Y., Wise, S.E., 1982. SERATRA: User's manual for the instream sediment–contaminant transport model. Pacific Northwest Laboratory, Battelle-Northwest, Richland, Wash *Technical Rep. No. PB-83e122739*.
Papanicolaou, A.T.N., Elhakeem, M., Krallis, G., Prakash, S., Edinger, J., 2008. Sediment transport modeling review—current and future developments. Journal of hydraulic engineering 134 (1), 1–14. doi:10.1061/(ASCE)0733-9429(2008)134:1(1).
Passalacqua, A., Laurent, F., Madadi-Kandjani, E., Heylmun, J.C., Fox, R.O., 2018. An open-source quadrature-based population balance solver for OpenFOAM. Chemical Engineering Science 176, 306–318. doi:10.1016/j.ces.2017.10.043.
Radović, I., Sobol, I.M., Tichy, R.F., 1996. Quasi-Monte Carlo methods for numerical integration: Comparison of different low discrepancy sequences. Monte Carlo Methods and Applications 2 (1), 1–14. doi:10.1515/mcma.1996.2.1.1.
Scott, W.T., 1968. Analytic studies of cloud droplet coalescence I. Journal of the atmospheric sciences 25 (1), 54–65. doi:10.1175/1520-0469(1968)025⟨0054:ASOCDC⟩2.0.CO;2.
Shen, X., Maa, J.P.Y., 2015. Modeling floc size distribution of suspended cohesive sediments using quadrature method of moments. Marine Geology 359, 106–119. doi:10.1016/j.margeo.2014.11.014.
Shen, X., Maa, J.P.Y., 2016. Numerical simulations of particle size distributions: Comparison with analytical solutions and kaolinite flocculation experiments. Marine Geology 379, 84–99. doi:10.1016/j.margeo.2016.05.014.
Shen, X., Maa, J.P.-Y., 2017. Floc size distributions of suspended kaolinite in an advection transport dominated tank: measurements and modeling. Ocean Dynamics 67, 1495–1510. doi:10.1007/s10236-017-1097-5.
Shen, X., Lee, B.J., Fettweis, M., Toorman, E.A., 2018a. A tri-modal flocculation model coupled with TELEMAC for estuarine muds both in the laboratory and in the field. Water research 145, 473–486. doi:10.1016/j.watres.2018.08.062.
Shen, X., Toorman, E.A., Lee, B.J., Fettweis, M., 2018b. Biophysical flocculation of suspended particulate matters in Belgian coastal zones. Journal of Hydrology 567, 238–252. doi:10.1016/j.jhydrol.2018.10.028.
Shen, X., Toorman, E.A., Lee, B.J., Fettweis, M., 2019. An approach to modeling biofilm growth during the flocculation of suspended cohesive sediments. Journal of Geophysical Research: Oceans 124 (6), 4098–4116. doi:10.1029/2018JC014493.
Shiea, M., Buffo, A., Vanni, M., Marchisio, D., 2020. Numerical Methods for the Solution of Population Balance Equations Coupled with Computational Fluid Dynamics. Annual review of chemical and biomolecular engineering 11, 339–366. doi:10.1146/annurev-chembioeng-092319-075814.
Shin, H.J., Son, M., Lee, G.-h., 2015. Stochastic flocculation model for cohesive sediment suspended in water. Water 7 (5), 2527–2541. doi:10.3390/w7052527.
Singh, M., Vuik, K., Kaur, G., Bart, H.-J., 2019. Effect of different discretizations on the numerical solution of 2D aggregation population balance equation. Powder Technology 342, 972–984. doi:10.1016/j.powtec.2018.10.028.
Singhee, A., Rutenbar, R.A., 2010. Why quasi-monte carlo is better than monte carlo or latin hypercube sampling for statistical circuit analysis. IEEE Transactions on Computer-Aided Design of Integrated Circuits and Systems 29 (11), 1763–1776. doi:10.1109/TCAD.2010.2062750.
Smith, M., Matsoukas, T., 1998. Constant-number Monte Carlo simulation of population balances. Chemical Engineering Science 53 (9), 1777–1786. doi:10.1016/S0009-2509(98)00045-1.
Smoluchowski, M., 1917. Versuch einer mathematischen Theorie der Koagulationskinetik kolloider Lösungen. Zeitschrift für Physikalische Chemie 92, 129–168 *in German*.
Sobol', I.y.M., 1967. On the distribution of points in a cube and the approximate evaluation of integrals. USSR Computational Mathematics and Mathematical Physics 7 (4), 86–112. doi:10.1016/0041-5553(67)90144-9.
Sobol, I.M., 1998. On quasi-monte carlo integrations. Mathematics and computers in simulation 47 (2-5), 103–112. doi:10.1016/S0378-4754(98)00096-2.
Son, M., Hsu, T.J., 2008. Flocculation model of cohesive sediment using variable fractal dimension. Environmental Fluid Mechanics 8 (1), 55–71. doi:10.1007/s10652-007-9050-7.
Son, M., Hsu, T.J., 2009. The effect of variable yield strength and variable fractal dimension on flocculation of cohesive sediment. Water Research 43 (14), 3582–3592. doi:10.1016/j.watres.2009.05.016.
Song, Y., Haidvogel, D., 1994. A semi-implicit ocean circulation model using a generalized topography-following coordinate system. Journal of Computational Physics 115 (1), 228–244. doi:10.1006/jcph.1994.1189.
Spicer, P.T., Pratsinis, S.E., 1996. Coagulation and fragmentation: Universal steady-state particle-size distribution. AIChE Journal 42 (6), 1612–1620. doi:10.1002/aic.690420612.
Su, J., Gu, Z., Li, Y., Feng, S., Xu, X.Y., 2008. An adaptive direct quadrature method of moment for population balance equations. AIChE Journal 54 (11), 2872–2887. doi:10.1002/aic.11599.
Su, J., Gu, Z., Xu, X.Y., 2009. Advances in numerical methods for the solution of population balance equations for disperse phase systems. Science in China Series B: Chemistry 52, 1063–1079. doi:10.1007/s11426-009-0164-2.
Tang, Y., Matsoukas, T., 1997. A New Monte Carlo Methods for Simulations of Agglomeration and Grinding. In: Fine Powder Processing Technology: Proceedings of the Fine Powder Processing Conference Sept 1997 Penn State, p. 243.
Tolhurst, T.J., Black, K.S., Shayler, S.A., Mather, S., Black, I., Baker, K., Paterson, D.M., 1999. Measuring the in situ Erosion Shear Stress of Intertidal Sediments with the Cohesive Strength Meter (CSM). Estuarine, Coastal and Shelf Science 49 (2), 281–294. doi:10.1006/ecss.1999.0512.
Toorman, E.A., 2012. Large-scale modeling of fine-grained sediment transport. Can we do any better? Actes des XIIième Journées Nationales Génie Côtier–Génie Civil (avec participation internationale 1, 491–502.
Tran, D., Strom, K., 2017. Suspended clays and silts: Are they independent or dependent fractions when it comes to settling in a turbulent suspension? Continental Shelf Research 138, 81–94. doi:10.1016/j.csr.2017.02.011.
Tran, D., Strom, K., 2019. Floc sizes and resuspension rates from fresh deposits: Influences of suspended sediment concentration, turbulence, and deposition time. Estuarine, Coastal and Shelf Science 229, 106397, . doi:10.1016/j.ecss.2019.106397.
Tsai, C.H., Hwang, S.C., 1995. Flocculation of sediment from the Tanshui River estuary. Marine and freshwater research 46 (1), 383–392. doi:10.1071/MF9950383.
Verney, R., Lafite, R., Brun-Cottan, J.C., Le Hir, P., 2011. Behaviour of a floc population during a tidal cycle: Laboratory experiments and numerical modelling. Continental Shelf Research 31 (10), S64–S83. doi:10.1016/j.csr.2010.02.005.
Walstra, D.J., van Rijn, L.C., Aarninkhof, S.G., 1998. Sand transport at the lower shoreface of the Dutch coast. Technical Rep. Z 2378.
Wang, C., Yuen, A.C.Y., Chan, Q.N., Chen, T.B.Y., Yang, W., Cheung, S.C.P., Yeoh, G.H., 2020. Characterisation of soot particle size distribution through population balance approach and soot diagnostic techniques for a buoyant non-premixed flame. Journal of the Energy Institute 93 (1), 112–128. doi:10.1016/j.joei.2019.04.004.
Wang, X., Hickernell, F.J., 2000. Randomized halton sequences. Mathematical and Computer Modelling 32 (7-8), 887–899. doi:10.1016/S0895-7177(00)00178-3.
Wang, X., Sloan, I.H., 2011. Quasi-Monte Carlo methods in financial engineering: An equivalence principle and dimension reduction. Operations Research 59, 80–95. doi:10.1287/opre.1100.0853.
Warren, I.R., Bach, H., 1992. MIKE 21: a modelling system for estuaries, coastal waters and seas. Environmental Software 7 (4), 229–240. doi:10.1016/0266-9838(92)90006-P.
Winterwerp, J.C., 1998. A simple model for turbulence induced flocculation of cohesive sediment. Journal of Hydraulic Research 36 (3), 309–326. doi:10.1080/00221689809498621.
Winterwerp, J.C., 1999. On the dynamics of high-concentrated mud suspensions. Delft University of Technology, Netherlands Ph.D.Dissertation.
Xu, Z., Zhao, H., Zheng, C., 2014. Fast Monte Carlo simulation for particle coagulation in population balance. Journal of Aerosol Science 74, 11–25. doi:10.1016/j.jaerosci.2014.03.006.
Xu, Z., Zhao, H., Zhao, H., 2017. CFD-population balance Monte Carlo simulation and numerical optimization for flame synthesis of TiO2 nanoparticles. Proceedings of the Combustion Institute 36 (1), 1099–1108. doi:10.1016/j.proci.2016.07.008.
Zhang, J.-F., Zhang, Q.-H., 2011. Lattice Boltzmann simulation of the flocculation process of cohesive sediment due to differential settling. Continental Shelf Research 31 (10), S94–S105. doi:10.1016/j.csr.2010.03.009.

Zhang, J.-F., Zhang, Q.-H., Maa, J.P.Y., Qiao, G.-Q., 2013. Lattice Boltzmann simulation of turbulence-induced flocculation of cohesive sediment. Ocean Dynamics 63 (9), 1123–1135. doi:10.1007/s10236-013-0646-9.

Zhang, Y., Ren, J., Zhang, W., 2020. Flocculation under the control of shear, concentration and stratification during tidal cycles. Journal of Hydrology 586, 124908, . doi:10.1016/j.jhydrol.2020.124908.

Zhao, H., Kruis, F.E., Zheng, C., 2011. Monte Carlo simulation for aggregative mixing of nanoparticles in two-component systems. Industrial & engineering chemistry research 50 (18), 10652–10664. doi:10.1021/ie200780q.

Zhao, H., Zheng, C., 2013. A population balance-Monte Carlo method for particle coagulation in spatially inhomogeneous systems. Computers & Fluids 71, 196–207. doi:10.1016/j.compfluid.2012.09.025.

Zhao, K., Vowinckel, B., Hsu, T.J., Köllner, T., Bai, B., Meiburg, E., 2020. An efficient cellular flow model for cohesive particle flocculation in turbulence. Journal of Fluid Mechanics 889. doi:10.1017/jfm.2020.79.

Ziff, R.M., McGrady, E.D., 1985. The kinetics of cluster fragmentation and depolymerisation. Journal of Physics A: Mathematical and General 18 (15), 3027–3037.